DOWN CONVERSION AND FILTERING OF MICROWAVE SIGNALS IN OPTICAL DOMAIN

A THESIS SUBMITTED TO
THE GRADUATE SCHOOL OF NATURAL AND APPLIED SCIENCES
OF
MIDDLE EAST TECHNICAL UNIVERSITY

BY

GÖKHUN SELÇUK

IN PARTIAL FULFILLMENT OF THE REQUIREMENTS
FOR
THE DEGREE OF MASTER OF SCIENCE
IN
ELECTRICAL AND ELECTRONICS ENGINEERING

MAY 2008

Approval of the thesis:

DOWN CONVERSION AND FILTERING OF MICROWAVE SIGNALS IN OPTICAL DOMAIN

submitted by **GÖKHUN SELÇUK** in partial fulfillment of the requirements for the degree of Master of Science **in Electrical and Electronics Engineering Department, Middle East Technical University** by,

Prof. Dr. Canan ÖZGEN _____
Dean, Graduate School of **Natural and Applied Sciences**

Prof. Dr. İsmet ERKMEN _____
Head of Department, **Electrical and Electronics Engineering**

Assist. Prof. Dr. A. Behzat ŞAHİN _____
Supervisor, **Electrical and Electronics Engineering Dept., METU**

Examining Committee Members:

Prof. Dr. Canan TOKER _____
Electrical and Electronics Engineering Dept., METU

Assist. Prof. Dr. A. Behzat ŞAHİN _____
Supervisor, Electrical and Electronics Engineering Dept., METU

Prof. Dr. Gönül Turhan SAYAN _____
Electrical and Electronics Engineering Dept., METU

Assoc. Prof. Dr. Şimşek DEMİR _____
Electrical and Electronics Engineering Dept., METU

Ms. Sinan KURT _____
Engineer, ASELSAN A.Ş.

Date: _____

I hereby declare that all information in this document has been obtained and presented in accordance with academic rules and ethical conduct. I also declare that, as required by these rules and conduct, I have fully cited and referenced all material and results that are not original to this work.

Name, Last name :

Signature :

ABSTRACT

DOWN CONVERSION AND FILTERING OF MICROWAVE SIGNALS IN OPTICAL DOMAIN

Gökhun SELÇUK
M.S., Department of Electrical and Electronics Engineering
Supervisor: Assist. Prof. Dr. A.Behzat Şahin

May 2008, 77 Pages

Processing of microwave signals in electrical domain introduces many difficulties especially when the frequency of the signal is increased beyond several GHz. Electromagnetic interference (EMI) and frequency depended losses can be given as examples to these difficulties. Photonic processing of microwave signals, however, is immune to these problems since optical components such as fiber cables, lasers, optical modulators and photodetectors are both immune to EMI and have wide bandwidths. This thesis deals with down conversion of a microwave signal using a Mach-Zender modulator and filtering unwanted harmonics using a photonic filter.

Keywords: Photonic signal processing, electromagnetic interference, fiber cable, Mach-Zender modulator, harmonics

ÖZ

MİKRODALGA SİNYALLERİN OPTİK ALANDA ALT ÇEVRİMLENMESİ VE FİLTRELENMESİ

Yüksek Lisans, Elektrik Elektronik Mühendisliği Bölümü
Tez Yöneticisi: Yrd. Doç. Dr. A. Behzat Şahin

Mayıs 2008, 77 Sayfa

Mikrodalga sinyallerin elektrik alanında işlenmesi, özellikle sinyalin frekansı birkaç GHz'in üzerine çıktığında, birçok güçlüğü beraberinde getirir. Elektromanyetik enterferans (EME) ve frekansa bağlı kayıplar bu güçlüklerin nedenleri olarak örnek gösterilebilir. Mikrodalga sinyallerin fotonik alanda işlemlenmesi ise; fiber kablolar, laserler, optik modulatörler, ve fotodetektörler gibi optik elemanların hem elektromanyetik enterferansa karşı duyarlı olmaması hem de geniş bantlı malzemeler olmaları nedeniyle bu güçlüklere karşı bağışıktır. Bu tezde bir mikrodalga sinyalin Mach-Zender modulator kullanılarak alt çevrimlenmesi gerçekleştirilmiş ve istenmeyen harmonikler bir fotonik filtre tarafından filtrelenmiştir.

Anahtar Kelimeler: Fotonik sinyal işlenmesi, elektromanyetik enterferans, fiber kablo, Mach-Zender modülatör, harmonikler

To my father

ACKNOWLEDGEMENTS

I am very grateful to my supervisor Assist. Prof. Dr. A. Behzat Şahin for his guidance, friendly encouragement and valuable recommendations.

I would like to express my thanks to Abidin Taşkıran for his help in the workplace. I am grateful to him and my colleagues for their understanding and moral support.

I would like to express special thanks to my family and my fiancée for their moral support and encouragement to complete the work.

TABLE OF CONTENTS

ABSTRACT ……IV
ÖZ……V
ACKNOWLEDGEMENTS...……...……VII
TABLE OF CONTENTS……VIII
LIST OF TABLES……..……XI
LIST OF FIGURES……...……XII
LIST OF ABBREVIATIONS……..……XIV
CHAPTERS
1.INTRODUCTION... …….....1
2. MICROWAVE PHOTONIC FILTERS……...……4
2.1 Characteristics of Fiber Cables……..…..……4
2.1.1 Fiber Loss….……4
2.1.2 Fiber Dispersion……...……6
2.1.3 Fiber Linearity…….……7
2.2 Filter Design Using Fiber Delay Lines…….……..……7
2.3 Coherent Regime and Incoherent Regime.....12
2.4 Limitations in Designing Photonic Microwave Filters……15
2.4.1 Optical Limitations……15
2.4.1.1 Optical Sources of Noise……15
2.4.1.2 Optically Induced Nonlinearities……17
2.4.1.3 Spectral Periodicity…….……17
2.4.1.4 Positivity of Tap Coefficients…….……18
2.4.1.5 Limited Spectral Period……..……18
2.4.1.6 Tunability……18
2.4.2 Electrical Sources of Performance Limitations……19
2.4.2.1 Gain…….19
2.4.2.2 Electrical Sources of Noise and Noise Figure….19
2.4.2.3 Linearity and Intermodulation Distortion……....21
2.5 Implementations of Photonic Filters ……...24

2.5.1 Single Source Microwave Photonic Filters……25
2.5.2 Multiple Source Microwave Photonic Filters ……27
2.5.3 Implementation of Negative Taps…...……..28
2.6 Practically Implemented Filters……29
2.6.1 The Finite Impulse Response Filter ……29
2.6.2 The Infinite Impulse Response Filter……32
3. THE PHOTODETECTOR AND THE LASER……36
3.1 The Photodetector……..……36
3.1.1 The Quantum Efficiency ……36
3.1.2 The Responsivity……37
3.1.3 Bandwidth and Capacitance……38
3.1.4 The Noise Equivalent Power……38
3.1.5 The Spectral Response ……38
3.2 The PIN Diode……39
3.3 The Laser……40
4. HARMONIC GENERATION USING LiNbO3 OPTICAL MODULATOR...43
4.1 Theory of Operation……43
4.2 The Structure of Mach-Zender Modulator……46
4.3 Generation of Harmonics……47
4.4 Practical Setup ……49
4.4.1 The Linearity of Generators ……50
4.4.2 The Linearity of Optical Detector ……52
4.5 Single Tone Modulation ……53
4.5.1 Fundamental Term ……55
4.5.2 Second Harmonic ……56
4.5.3 Third Harmonic ……56
4.5.4 The Behaviour at Another Signal Level ……57
4.5.5 The Spectrum ……58
4.6 Two Tone Modulation ……59
4.6.1 Fundamental Term ……61
4.6.2 Difference Term ……62
4.6.3 The Second Harmonic ……62
4.6.4 The Spectrum ……63

5. CONCLUSIONS ……...……68
REFERENCES ……..……71
APPENDIX ……74

LIST OF TABLES

Table 3.1 Semiconductor materials and respective wavelength ranges ……39

LIST OF FIGURES

Figure 1.1 Traditional RF signal processing method…… 1

Figure 1.2 Optical domain RF signal processing method……..2

Figure 2.1 Loss in the Fiber versus Wavelength……..…..5

Figure 2.2 Loss in the Fiber versus modulating frequency……..……..6

Figure 2.3 The impulse response of a microwave filter……..……...8

Figure 2.4 (a) schematic of an FIR photonic microwave filter (b) schematic of an IIR photonic microwave filter……..…….9

Figure 2.5 Two FIR filters with different number of taps……...11

Figure 2.6 The spectrum of a typical photonic filter and the related parameters……...11

Figure 2.7 the dependence of PIIN to optical input power……..17

Figure 2.8 The propagation path of the RF signal……...19

Figure 2.9 Parameters for the measurement of nonlinearity a) spurious free dynamic range b) third order intercept point….....……..24

Figure 2.10 A coherence free single source photonic filter……...25

Figure 2.11 A hybrid filter that utilizes an active medium to increase the number of taps……..26

Figure 2.12 A MSMPF based on laser array……..28

Figure2.13 MSMPF utilizing dispersive medium…….29

Figure 2.14 Implementation of negative taps using differential detection……30

Figure 2.15 The setup of the two tap fir filter……30

Figure 2.16 the response of fir filter……..31

Figure 2.17 Noise contributions in two-tap filter……...32

Figure 2.18 The schematic of the IIR filter……33

Figure 2.19 the coupling at the combiner/splitter……..33

Figure 2.20 the response of the IIR filter a) the plot taken from network

analyzer b) simulated response in matlab…….....…35
Figure 2.21 Filter Response for κ = 0.33 ……...……...35
Figure 3.1 Responsivity curve of a semiconductor optical detector……37
Figure 3.2 The Structure of a PIN diode……..39
Figure 3.4 Laser Structure……40
Figure 3.5 Three Level Laser System……..41
Figure 3.6 The Spectrum of Laser Output……...……42
Figure 4.1 The direction of the applied filed and polarization ……45
Figure 4.2 The structure of Mach-Zender Modulator……..46
Figure 4.3 The response of modulator……48
Figure 4.4 Setup to create and analyze harmonics……50
Figure 4.5 the response of isolator……...51
Figure 4.6 the output of the combiner before and after the insertion of isolators……52
Figure 4.7 Simulation setup to analyze the system……..54
Figure 4.8 Fundamental term versus DC Bias……56
Figure 4.9 Second harmonic versus DC Bias……...56
Figure 4.10 Third harmonic versus DC Bias…….……57
Figure 4.11 Harmonics for 10 dBm and 15 dBm inputs……59
Figure 4.12 Spectrum at the output of the modulator……60
Figure 4.13 Simulation setup to analyze the two tone system……...61
Figure 4.13 Fundamental term (two-tone) versus DC Bias……...62
Figure 4.14 Difference term versus DC Bias……63
Figure 4.15 Second harmonic (two-tone) versus DC Bias……63
Figure 4.16 The spectrum for two tone modulation a) simulation b) output of spectrum analyzer……...64
Figure 4.17 The schematic and response curves for the combining Circuitry……..67
Figure 4.18 Output Signal level versus a) LO Level b) Input Signal Level….67
Figure 4.19 The picture of the setup……..……68

LIST OF ABBREVIATIONS

EMI	Electromagnetic Interference
RF	Radio Frequency
IF	Intermediate Frequency
DSP	Digital Signal Processing
RoF	Radio over Fiber
SBS	Stimulated Brillouin Scattering
SRS	Stimulated Raman Scattering
IIR	Infinite Impulse Response
FIR	Finite Impulse Response
FSR	Free Spectral Range
MSSR	Main to Secondary Sidelobe Ratio
RIN	Relative Intensity Noise
PIIN	Phase Induced Intensity Noise
NF	Noise Figure
IP3	Third Order Intercept Point
IMD	Intermodulation Distortion
SFDR	Spurious Free Dynamic Range
SSMPF	Single Source Microwave Photonic Filter
MSMPF	Multiple Source Microwave Photonic Filter
EDF	Erbium Doped Fiber
NEP	Noise Equivalent Power
LO	Local Oscillator

CHAPTER 1

INTRODUCTION

Utilization of inherent and unique properties of photonic devices in processing of microwave signals offer several advantages compared to the classical processing methods and is subject to constant research over the last 25 years. The area of research has emerged as a new discipline known as Microwave Photonics [1].

In the classical approach, which is illustrated in Figure 1, the microwave signal from an RF source is captured by means of an antenna and fed to an RF processing block which operates in electrical domain. This block applies filtering, amplification and down-conversion functions and its main task is to transmit the signal from the antenna to the IF section or DSP, without adding much noise and distortion. Also the RF section should filter some unwanted frequencies which degrade the performance of the receiver by adding noise, saturating low noise amplifier, falling to the signal band after mixing etc.

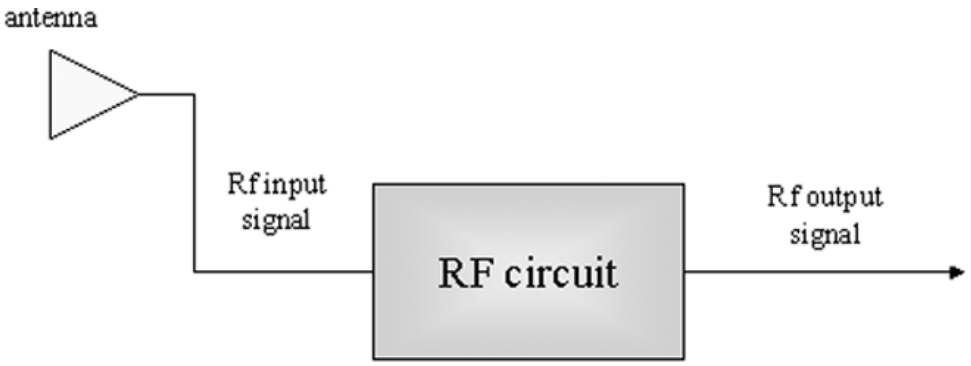

Figure 1.1 Traditional RF signal processing method

Although commercially accepted and applied, the classical approach has several disadvantages especially when the frequency of the receiving signal is increased beyond several GHz. These disadvantages include electromagnetic interference (EMI), frequency dependent losses and the requirement to change the design when the receiver band is changed [2].

The above problems, known as the electronic bottleneck, can be solved by introducing photonic technology in to the system, which is shown in Figure 2.

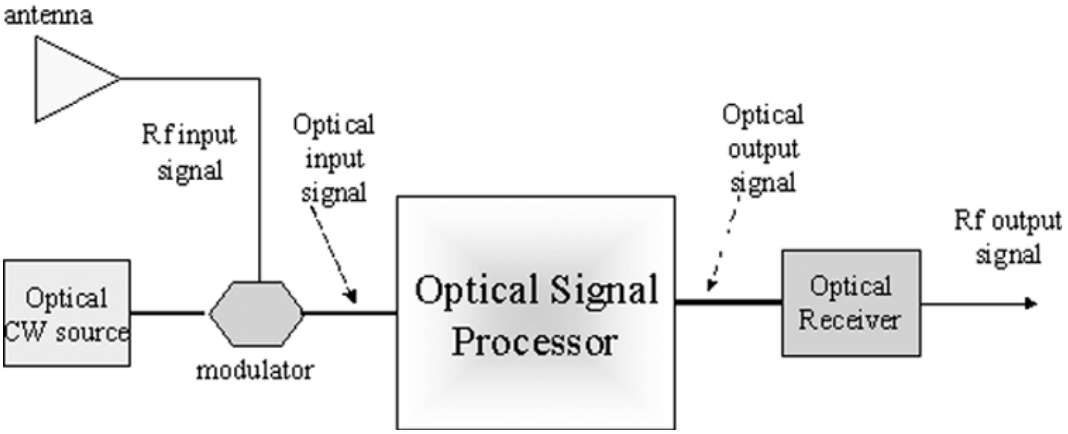

Figure 1.2 Optical domain RF signal processing method

In this approach the RF signal received by the antenna is fed to the modulation input of an optical modulator to be processed in the optical domain. Filtering, amplification and even down conversion tasks can be applied in this domain. The output of the optical signal processor is fed to an optical receiver to be converted back to the electrical domain.

This structure is immune to electromagnetic interference since fiber lines are inherently immune to EMI, also fiber lines introduce low-loss which is a critical issue in designing filters. Large bandwidths (more than 40 GHz) of the optical modulator and the optical receiver allow flexible designs without spending much effort.

Following outline is followed throughout this work. In Chapter 2 the principles and structures of microwave filters will be presented, the principles of operation of the lasers and photodetectors is introduced in Chapter 3. Chapter 4 deals with the down-conversion unit which utilizes the optical modulator as the nonlinear device to generate harmonics. This chapter is followed by the conclusions section and the appendix part which gives important pages of the datasheets of the components used.

CHAPTER 2

MICROWAVE PHOTONIC FILTERS

A microwave photonic filter is a photonic signal processing structure whose task is, like an ordinary microwave filter, to pass the desired signal without much loss and to attenuate the unwanted signals. For example the microwave photonic filters are of interest in radio over fiber (RoF) systems both for channel selection and the channel rejection applications [3].

The use of optical delay lines for optical signal processing applications was first purposed by Wilner and van den Heuvel in 1976 [4]. The fiber delay lines are attractive because they both have low loss and dispersion.

This chapter covers the principles of operation of photonic filters with an introduction to fiber cable properties. This section is followed by a section presenting the general structures and performance characteristics of photonic filters. Finally two filters are constructed and their responses are analyzed

2.1 Characteristics of Fiber Cables

Among the several characteristic parameters of the fiber-delay lines the two important ones for the use in the filter design are the loss and the dispersion of the optical fiber

2.1.1 Fiber Loss:

Attenuation of the optical power transmitted through the fiber determines the feasible length of the optical fiber used in a specific application [5]. The loss in

fibers is both due to the absorption and the scattering mechanisms.

The absorption is due to the light-matter interactions and dissipated as heat in the core and the cladding. For fused silica glass (SiO_2) the two major absorption bands are the infrared absorption band (caused by the interaction of photons with molecular vibrations) and the ultraviolet absorption band (caused by the stimulation of electron transitions within the glass). A third absorption mechanism is the OH absorption caused by the water vapor in the glass during the fabrication process [5].

The scattering in the fiber has two important sources. The first is the Rayleigh scattering which is caused by the interaction of light with the impurities in the fiber for which the impurity atoms have sizes much smaller than the wavelength of the optical carrier. Another major scattering mechanism is the Mie scattering in which the impurity atoms have sizes comparable the wavelength of the optical carrier [6]. The transmission characteristics of the fiber are given in Figure 2.1 and the loss as a function of the modulating RF frequency is given in Figure 2.2.

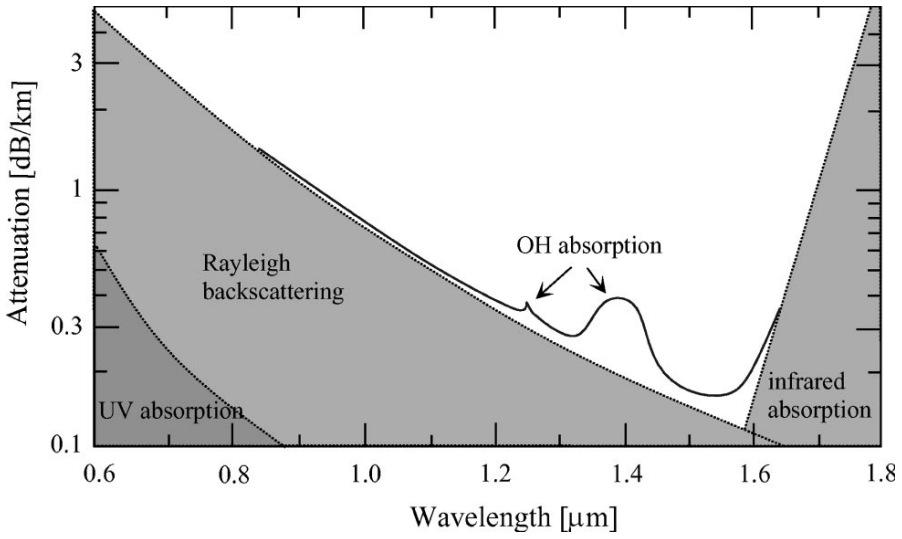

Figure 2.1 Loss in the Fiber versus Wavelength

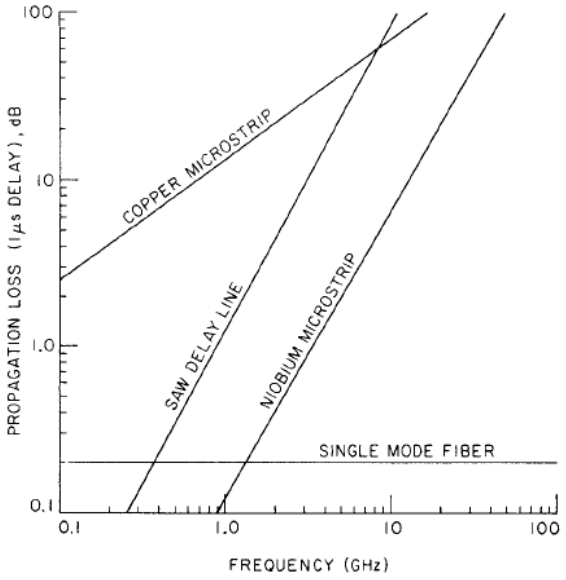

Figure 2.2 Loss in the Fiber versus modulating frequency

From Figure 2.1, it is evident that use of the fiber is restricted to about 1.5-1.6 μm to exhibit low loss. However this is not a problem for photonic filters since lasers at 1.55 μm are commercially available. Figure 2.2 plots the loss of fiber versus the modulating frequency, which is constant up to 100 GHz. This makes fiber attractive for the utilization as a delay line element [7].

Apart from the absorption and scattering losses in the fiber cable, the optical signal is also attenuated by the bending losses which are caused by the radiation at the bend points and connector losses introduced when connecting two cables or splicing them.

2.1.2 Fiber Dispersion:

A short pulse (wide frequency content) propagating through the fiber does not conserve its shape due to the several dispersion mechanisms in the fiber. This fact sets an upper limit to the bandwidth of the signal to be transmitted through the fiber. Among the many dispersion mechanisms the most important three are the modal dispersion, material dispersion and the waveguide dispersion.

The modal dispersion occurs in multimode fibers in which the group velocity of each mode is different. This type of dispersion is proportional to the fiber length and may be reduced by using graded index fiber. For single mode fibers this type of dispersion is eliminated.

The material dispersion is due to the change of the refractive index of the fiber with the change in frequency. This type of dispersion is also proportional to the fiber length and occurs in both single mode and multi mode fibers.

The waveguide dispersion occurs since the group velocity of a mode is dependent on the ratio of the power traveling in the core to the power traveling in the cladding. The core radius-wavelength ratio changes the ratio of power traveling in the core to the power traveling in the cladding. Thus the group velocities of the modes are wavelength dependent [5].

2.1.3 Fiber Linearity:

The loss and the dispersion mechanisms mentioned above are assumed to be linear processes. However at high optical power levels the fiber starts to become nonlinear due to some nonlinear loss and dispersion mechanisms.

The two nonlinear loss mechanisms are the Stimulated Brillouin Scattering (SBS) and the Stimulated Raman Scattering (SRS) which are introduced by the modulation of light by thermal molecular vibration within the fiber. Nonlinear dispersion is due to the intensity dependent refractive index at high power levels.

2.2 Filter Design Using Fiber Delay Lines

The principle of operation of a photonic microwave filter is similar to its electrical domain counterpart. The filter divides the incoming signal into N parts and applies different delay and weightings to each part before summation. The mathematical equivalent is given in Figure 2.3.

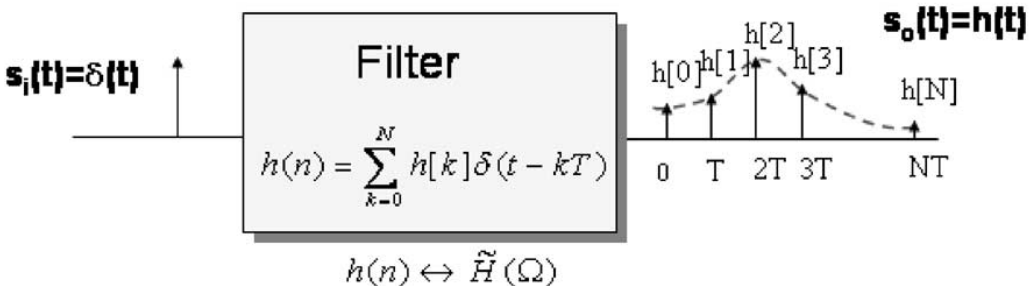

Figure 2.3 The impulse response of a microwave filter

Filters can be classified according to their impulse responses, a finite impulse response filter (FIR) use only current and past input samples (see Figure 2.4.a) and none of the filters previous output samples.(This is why they are also called as non-recursive filters).Given a finite duration signal the output of the filter has always finite nonzero duration. Infinite Impulse Response (IIR) filters are fundamentally different from the FIR filters in that practical IIR filters always require feedback (see Figure 2.4.b). Although FIR filter output depend on previous and current input samples, the IIR's output depend also on previous output samples. So if the IIR filter's input is a signal of finite duration the output still is infinite [8].

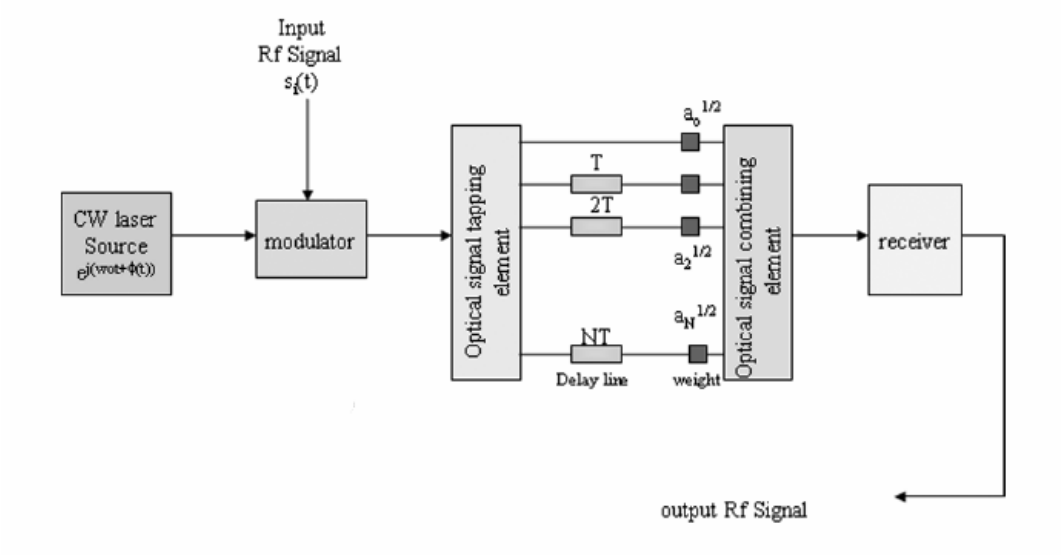

(a) FIR photonic microwave filter

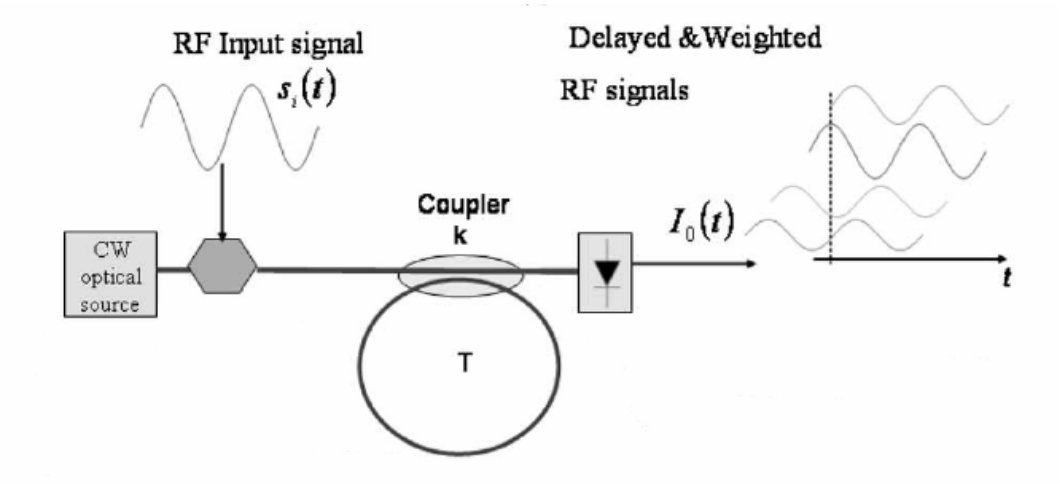

(b) IIR photonic microwave filter

Figure 2.4 (a) schematic of an FIR photonic microwave filter (b) schematic of an IIR photonic microwave filter

For an N-tap FIR filter the impulse response is given by

$$h(t) = \sum_{n=0}^{N} a_n \times \delta(t - nT) \tag{2.1}$$

where a_n is the weighting applied to the n^{th} component

t_n is the delay experienced by the n^{th} component

And the z transform of the impulse response is given by

$$H(z) = \sum_{n=1}^{N} a_n \times z^{-n} \tag{2.2}$$

For an input signal $s_i(t)$ the output signal $s_o(t)$ is the convolution of the input signal with the impulse response and is given by

$$s_o(t) = s_i(t) * h(t) = \sum_{n=1}^{N} a_n \times s_i(t - nT) \tag{2.3}$$

And for and IIR filter the equation relating the output signal to the input signal is given by the equation

$$s_o(t) = \sum_{n=1}^{N} a_n \times s_i(t - nT) + \sum_{k=1}^{M} b_k \times s_o(t - kT) \qquad (2.4)$$

So the z-transform of the impulse response of the filter is given by

$$H(z) = \frac{\sum_{n=1}^{N} a_n \times z^{-n}}{1 - \sum_{k=1}^{M} b_n \times z^{-n}} \qquad (2.5)$$

The above expression identifies a transfer function with a periodic spectral characteristics. The frequency period is known as the filters free spectral range (FSR) and is inversely proportional to the minimum delay length T, in the system. The full width half maximum value at the resonance point (the point where filter passes the signal with minimum attenuation) is denoted by $\Delta\Omega_{FWHM}$ [2]. The selectivity of the filter, given by the quality factor of the filter, is the ratio

$$Q = \frac{FSR}{\Delta\Omega_{FWHM}} \qquad (2.6)$$

The Q-factor of the filter is related to the number of taps used in the filter. For higher number of taps higher Q values is obtained. Recently Q-factor of 237 is reported for an FIR filter [9] and a Q factor of 938 is presented for an IIR filter [10]. Figure 2.5 shows two FIR filters with different number of taps. The dashed line has three taps with weighting 0.33 each and the solid line has 10 taps with weighting 0.1 each to normalize the power. Note the difference between the Q-factors of the filters.

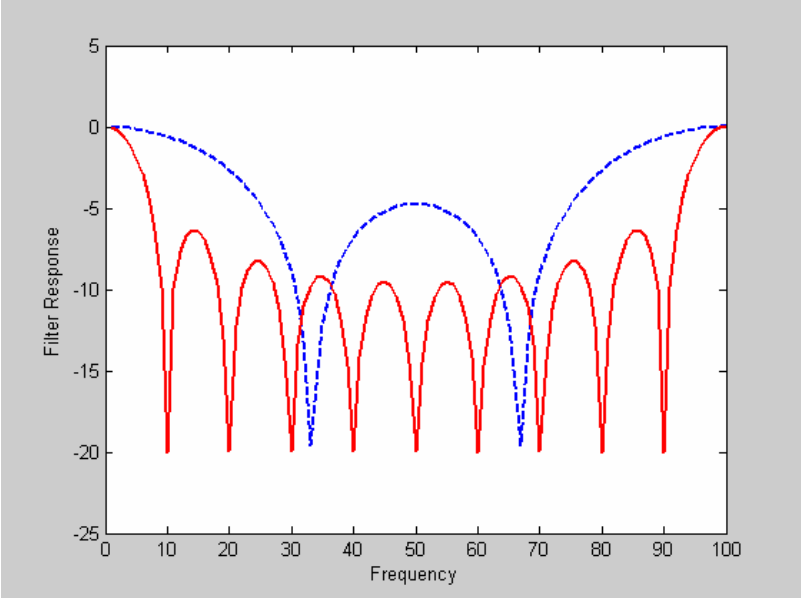

Figure 2.5 Two FIR filters with different number of taps

The main to secondary side lobe ratio (MSSR) value gives the attenuation at the side lobe relative to the attenuation in the main lobe. The plot concerning the parameters defined is given in Figure 7.

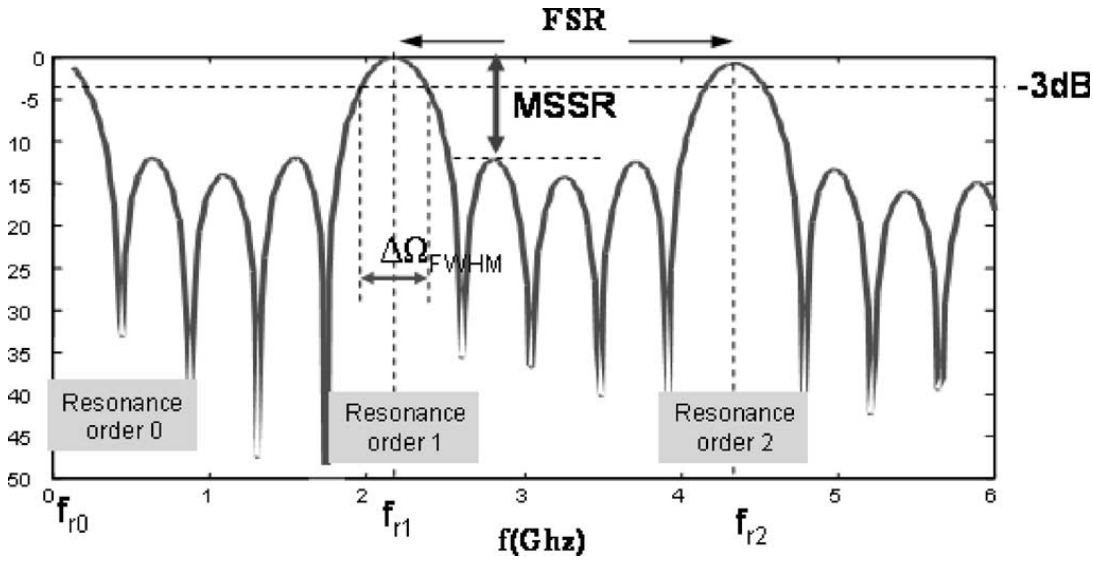

Figure 2.6 The spectrum of a typical photonic filter and the related parameters

2.3 Coherent Regime and the Incoherent Regime

Apart from the Finite Impulse Response and the Infinite Response classification, another way of classifying the filters concerns the operation regimes. The term coherent and incoherent stems from the summation process in the detector side.

Microwave photonic filters are schematically and operationally similar to the electrical delay line filters. Thus both analysis and design methods of classical delay line filters can be utilized for photonic filters. However there are some characteristics unique to photonic filters which one must take into account in analysis of these types of filters.

The unique property of these filters are due to the conversion processes from the electrical domain to the optical domain at the modulator side and due to the conversion process from the optical domain to the electrical domain at the detector side.

Optical modulators change their output light intensities by the applied voltage to their RF ports (a detailed analysis of the modulators is given in Chapter 4. Thus for and applied signal $s_i(t)$, the modulators output light intensity is given by

$$I_o(t) = k^* s_i(t)^* I_i \tag{2.7}$$

where I_i is the input light intensity to the modulator
k is a constant including the modulation index of the modulator at a given operating point
$s_i(t)$ is the applied input signal
and $I_o(t)$ is the output light intensity

For this intensity the electric field propagating through the fiber is given by

$$E_i(t) = \sqrt{kI_i}\sqrt{s_i(t)} \tag{2.8}$$

And the signal at the detector is the sum of the delayed samples

$$E_o(t) = \sqrt{kI_i} \times \sum_{n=1}^{N} \sqrt{a_n s_i(t-nT)} \exp\left(j\left(w_o(t-rT) + \varphi(t-rT)\right)\right) \quad (2.9)$$

Optical detectors do not respond to the carrier frequency and respond only to the input power (detailed analysis of the detector is given in Chapter 3). So the output current of the detector is

$$I_{\text{det}} = \Re\left\langle \left|E_o(t)\right|^2 \right\rangle \quad (2.10)$$

Where $\Re$ is the responsitivity of the detector which will be mentioned in Chapter3.

And putting the value of the electric field at the input of the detector, one obtains the output current of the detector as,

$$\begin{aligned} I_{\text{det}} = \; & \Re I_i \sum_{n=1}^{N} |a_n| s_i(t-nT) \\ & + \Re I_i \sum_{n=1}^{N} \sum_{k \neq n}^{N} \sqrt{a_n a_k^* s_i(t-nT) s_i(t-kT)} \times \Gamma\left((n-k)T\right) \end{aligned} \quad (2.11)$$

where the $\Gamma\left((n-k)T\right)$ term concerning the optical phase at the input of the detector

Thus the output signal is composed of two terms. One is the incoherent term whose value is linearly dependent on the input value and a coherent term which violates the linearity of the system.

The $\Gamma((n-k)T)$ term can be modeled by $\exp\left(-\frac{|(k-n)T|}{\tau_{coh}}\right)$ [11]. Where $\tau_{coh} = \frac{1}{\pi\Delta\nu}$ is the source coherence time and $\Delta\nu$ is the linewidth of the laser which will be mentioned in Chapter3.

For the source coherence time much smaller than the minimum delay in the filter the equation reduces to

$$I_{\det} = \Re I_i \sum_{n=1}^{N} |a_n| s_i(t-nT) \tag{2.12}$$

which has liner transfer characteristic as inferred from the equation.

The filters operating in incoherent regime have many advantages over those which operate in coherent regime. Since the filter response does not dependent on the optical phase, perturbations on the phase do not effect the filter response and filter response is immune to environmental changes such a vibrations and perturbations in the temperature. The main drawback of the incoherent filters is that, the taps have always positive coefficients. Thus only a limited number of filter responses can be realized using incoherent filters.

For the coherence time comparable to the minimum delay in the structure the $\Gamma((n-k)T)$ term can be approximated by $\exp(jw_o(n-k)T)$ [11] and the output current of the detector is given by

$$\begin{aligned} I_{\det} = {} & \Re I_i \sum_{n=1}^{N} |a_n| s_i(t-nT) \\ & + \Re I_i \sum_{n=1}^{N} \sum_{k\neq n}^{N} \sqrt{a_n a_k^* s_i(t-nT) s_i(t-kT)} \times \exp(jw_o(n-k)T) \end{aligned} \tag{2.13}$$

It is evident from the formula that the output of the detector consists of a linear term (the incoherent term) and a coherent term which is sensitive to the phase of the optical signal. The main advantage of this type of filters is that the overall

tapping coefficient can now be made negative. However the response is strongly dependent on the environmental changes since small increments in the fiber length can cause large phase changes due to the high frequency of the optical carrier. Therefore it is very difficult to stabilize the response of these type of filters and coherent filters are not utilized in practice.

2.4 Limitations in Designing Photonic Microwave Filters

For practical realization of photonic microwave filters, there are a number of issues to be taken into account which limit the performance of these types of filters. The limitations may arise either in the optical domain or in the electrical domain thus these are analyzed in two subsections presented below.

2.4.1 Optical Limitations

Beside the advantages that microwave filters bring in solving electronic bottleneck in high frequency applications there are also some drawbacks introduced by the optical properties of these filters and are analyzed under the topic of optical limitations to microwave photonic filters.

The main limitations that appear in optical domain are the noise terms in the optical domain, optically induced nonlinearities, spectral periodicity, positivity of filter tap coefficients, limited spectral period and tunability.

2.4.1.1 Optical Sources of Noise:

Noise is an important concept in RF literature since it determines the minimum detectable signal for a receiver thereby also influences the dynamic range of the system which is defined to be the difference between the minimum and the maximum signal levels that the receiver architecture can handle.

Unfortunately, introduction of photonic filters to the receiver structure inserts some additional noise sources to the system. Two major sources of noise in the

optical domain are the laser relative intensity noise (RIN) and the phase induced intensity noise (PIIN).

The relative intensity noise (RIN) is the noise current at the output of the optical detector caused by the fluctuations at the output of the laser. The fluctuations can be resulted either from the vibrations of optical cavity or perturbations in the gain medium [13]. Although RIN is not dependent on the output power of the laser, the referred noise to the output of the optical detector is dependent on the optical power. The power spectral density of the noise at the detector side is given by

$$N_{RIN} = I_p^2 \times RIN, \; where \; I_p = \Re P_{opt} T_{opt}$$

where

P_{opt} is the optical output power of laser

T_{opt} is the loss (gain) of optical domain

RIN is the spectral density of noise at the output of laser

The most important noise source in microwave filters which dominates other noise mechanisms by far is the phase induced intensity noise (PIIN). In the discussion of coherent and incoherent regime of operation of optical filters, the equation relating the output of the filter to the input signal was derived and it was mentioned that use of coherent filters for practical applications are difficult due to the stability considerations. However even for incoherent regime of operation there exists some phase correlation between the samples that have experienced different delays.

For a given optical source, the number of optical taps and the weights of these taps that are combined determine the spectrum and level of the PIIN. For a given processor structure, the PIIN is also related to the coherence time of the optical source. Hence, the spectrum of the PIIN is a function of the topology of the processor and the coherence of the optical source [14]. The PIIN equation is rather involved and is not presented here. The spectral density shape of a two tap filter is presented in [15]. However it is important to mention that PIIN spectrum, like

the spectrum of RIN increases with the square of the input laser power as shown in Figure 2.7.

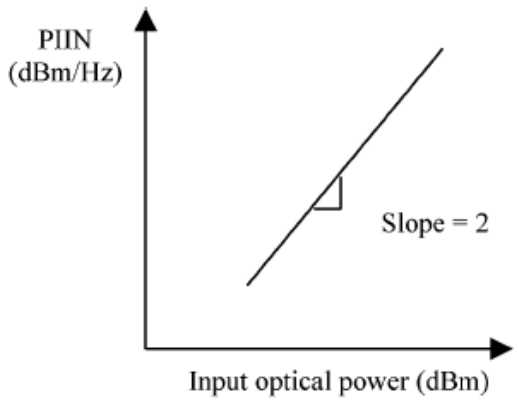

Figure 2.7 The dependence of PIIN to optical input power

Since the RF power also increase as the square of the optical power, the signal to noise ratio at the detector can not be increased by increasing the laser power.

2.4.1.2 Optically Induced Nonlinearities

Previously it was mentioned that for high optical power levels, the nonlinear absorption and scattering mechanisms start to degrade the linear response of the filter. These were due to the Stimulated Raman Scattering (SRS) and stimulated Brillouin Scattering(SBS). Also the nonlinearities arising during the electrical to optical conversion process and optical to electrical conversion process may also set limit to dynamic range at high optical powers.

2.4.1.3 Spectral Periodicity

The free spectral range (FSR) was defined previously as the repetition period of the response of the filter and is inversely proportional to the inverse of the minimum delay in the system. Thus the bandwidth of the RF signal to be

processed should not be larger than the FSR if single resonance response is required.

2.4.1.4 Positivity of Tap Coefficients

For incoherent filters the equation relating the detector current to the input signal was found to be

$$I_{\text{det}} = \Re I_i \sum_{n=1}^{N} |a_n| s_i(t - nT) \tag{2.14}$$

Since the detector responds to optical power and not to the optical phase, the coefficients in the above equation are inherently positive. This limits the variety of the filter responses that can be designed by using photonic technologies. Although some methods are introduced to implement filters with negative coefficients [16],[17] these introduce considerable complexity to the system.

2.4.1.5 Limited Spectral Period

It was mentioned previously that the response of photonic filters repeat themselves at a rate 1/T where T is the minimum delay in the filter. However, for incoherent filters the minimum delay time should be larger than the coherence length of the laser source. If this is not the case filter will suffer from both the nonlinear effects and the PIIN noise. This fact sets an upper limit to the minimum delay in the fiber thereby setting an upper limit to the FSR. In order to overcome this problem, filters utilizing more than one lasers are purposed [18],[19] since in this case correlation between the phases of the optical carriers is totally lost.

2.4.1.6 Tunability

The tunability refers to the ability of changing the response of the filter. In order to achieve this, the delay lengths of the filter should be changed. To provide

tunability switched delay line and high dispersion fibers utilizing multiple lasers are purposed [21].

2.4.2 Electrical Sources of Performance Limitations

Although the photonic microwave filter does achieve its task in optical domain, it may be considered as a black box with an electrical input at the RF port of the optical modulator and an electrical output at the optical detector side. Therefore photonic filters, like their electrical counterparts, are subject to some electrical performance criteria and limitations such as gain (loss), noise figure and intermodulation distortion.

2.4.2.1 Gain

The gain of a photonic filter can be found by simply pursuing the RF signal as it propagates through the filter. The three parts influencing the total gain of the filter are the electro-optic conversion, losses in the optical domain and the opto-electronic conversion which are shown in Figure 10.

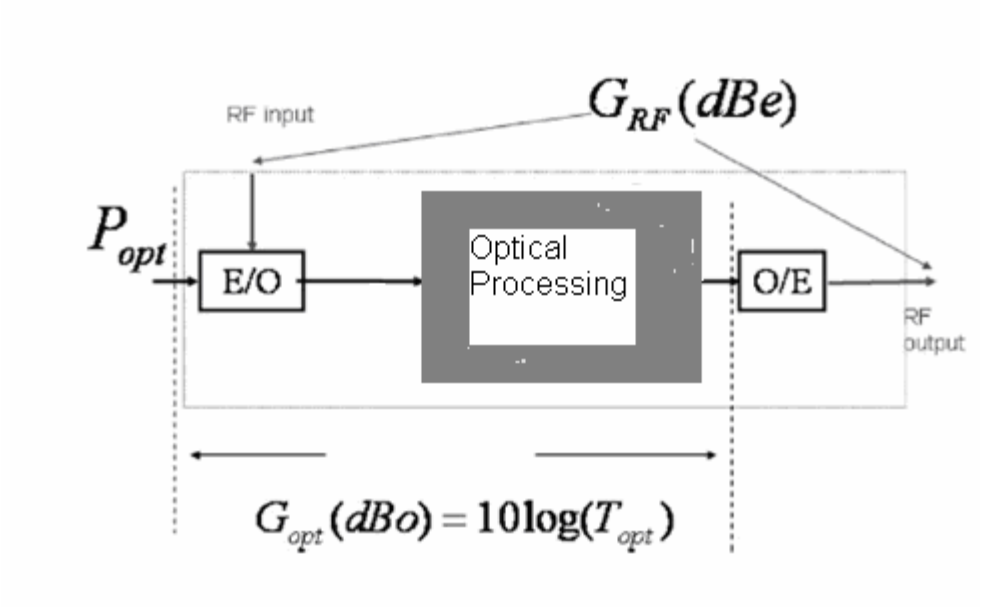

Figure 2.8 The propagation path of the RF signal

First the RF signal is used to modulate the output light intensity (power) of an optical modulator (A detailed analysis of the modulator is given in Chapter 4. The output light intensity of the modulator, assuming the operation at quadrature bias, as a function of the input RF voltage is given by the formula

$$I_{out} = I_{in} \frac{\pi \times V_{in}}{2V_{\pi}} \tag{2.15}$$

where I_{out} is the output light intensity

I_{in} is the input light intensity

V_{in} is the applied input signal

V_{π} is the voltage required to change modulators output intensity from its maximum value to its minimum value

For an input RF power of P_{in} to the modulator having the input impedance Z_o the peak value of the input voltage is $V_{in} = \sqrt{2P_{in} \times Z_o}$ and the modulator output intensity is given by

$$I_{out} = I_{in} \frac{\pi \times \sqrt{2P_{in} \times Z_o}}{2V_{\pi}} \tag{2.16}$$

If the loss in the optical path is L, then the intensity at the input of the optical detector is

$$I_{\det} = I_{in} L \frac{\pi \times \sqrt{2P_{in} \times Z_o}}{2V_{\pi}} \tag{2.17}$$

The output current of the detector is $\Re I_{\det}$ where $\Re$ is the responsivity of the detector. Thus the output power of the detector (assuming a load of Z_o) is given by

$$P_{out} = \left(\Re I_{\det}\right)^2 Z_o / 2 = \left(\frac{I_{in} \pi L Z_0}{2V_{\pi}} \Re \right)^2 P_{in} \tag{2.18}$$

And the total RF gain is

$$\frac{P_{out}}{P_{in}} = \left(\frac{I_{in} \pi L Z_0}{2V_\pi} \Re \right)^2 \tag{2.19}$$

Note that the gain is proportional to the square of the input light intensity, this fact is utilized to compensate both electrical and the optical losses since this method increases the gain without any external amplifiers.

2.4.2.2 Electrical Sources of Noise and Noise Figure

The two noise mechanisms are the shot noise and the thermal noise. The source of the shot noise is the quantized nature of the charge carriers. An average current of I_{avg} does not deliver always the same amount of electrons at a given differential time interval Δt. Rather the number of electrons delivered has a poissonian distribution which peaks at the value $I_{avg}\ \Delta t$. The statistical fluctuations of the received number of electrons results in shot noise with a power spectral density

$$N_{shot} = 2qI_p, \text{ where } I_p = \Re P_{opt} T_{opt} \tag{2.20}$$

The source of the thermal noise is the thermal agitation of charge carriers inside a conductor. This type of noise is independent of the applied voltage and its power spectral density is given by

$$N_{thermal} = \frac{4kT}{R} \tag{2.21}$$

Where k is the Boltzman constant
T is the temperature in Kelvin
R is the resistance value of the conductor

The noise figure of a two port is defined as the ratio of the total noise power at the

output port to the noise power at the output port due to the input noise only. Thus if the two port has a gain of G, assuming only thermal noise at the input port, the noise figure is given by

$$NF(dB) = 10\log_{10}\left(\frac{N_{out}}{\frac{4kT}{R}G}\right) \tag{2.22}$$

The total noise power of a photonic microwave filter is the sum of the noise terms defined in the previous section. Thus the noise figure of the filter is given by the expression

$$NF(dB) = 10\log_{10}\left(\frac{N_{RIN} + N_{shot} + N_{PIIN} + N_{th}}{\frac{4kT}{R}G}\right) \tag{2.23}$$

2.4.2.3 Linearity and Intermodulation Distortion

Except from the nonlinearities induced in the fibre at high levels of light intensities, there are other sources of nonlinearities introduced at different blocks of the filter. These are introduced mainly at the modulator during the electro-optical conversion, and at the detector during the opto-electronic conversion.

The nonlinearity in electro-optical modulator is the major source and limits the maximum level of the signal that the system can handle. The nonlinearity manifests itself as the harmonics introduced to the spectrum of the output signal. The performance parameters of the nonlinearity are the spurious free dynamic range and the IP3.

For linear operation of the modulator, it is biased at the quadrature point where the conversion efficiency of the fundamental term is maximum and second level

harmonic distortion are at their lowest levels. The third order harmonics are also the strongest harmonics at that biasing points.

A performance parameter regarding the third order nonlinearity is the IP3. IP3 is measured by applying two equal level signals at frequencies f_1 and f_2 to the nonlinear device and observing the intermodulation terms at $2f_2$-f_1 or $2f_1$-f_2 (see Figure 11 a). These are the most deleterious intermodulation products since they are very close to the signal bandwidth and cannot be filtered easily. The IP3 is a virtual point where the level of third order intermodulation product is equal to the fundamental term. Note that for every Db increment of the fundamental term, the third order intermodulation term increases by 3 Db [22]. IP3 is a virtual point since the saturation effects prevent the imd terms to reach the fundamental term.

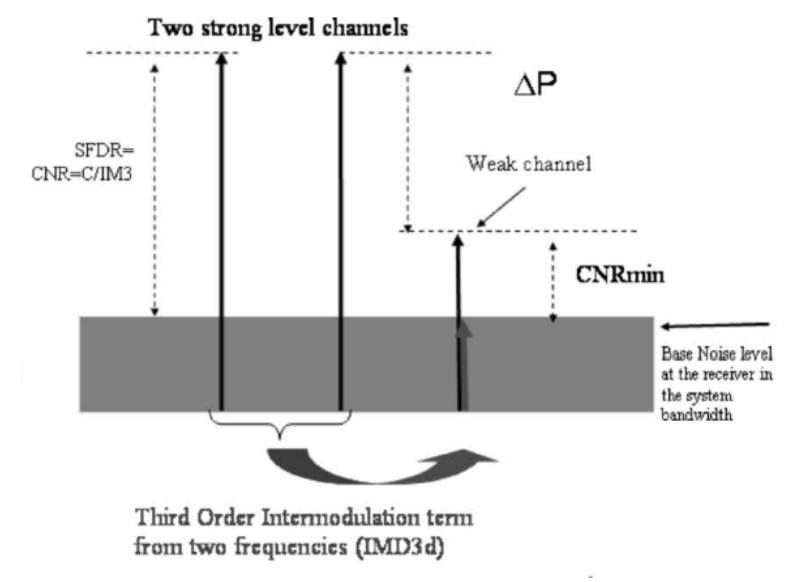

a) spurious free dynamic range

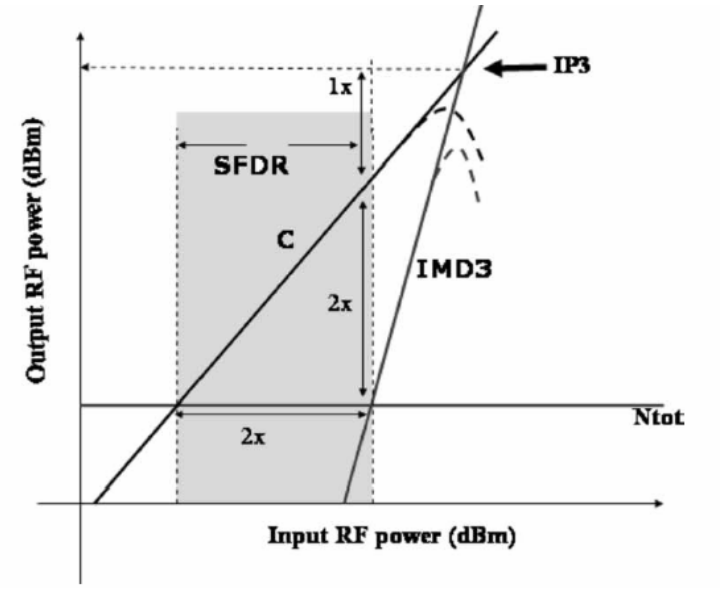

b) third order intercept point

Figure 2.9 Parameters for the measurement of nonlinearity a) spurious free dynamic range b) third order intercept point

The spurious free dynamic range (SFDR) is defined as the fundamental carrier to the two-tone third order intermodulation products just when the IMD3 product power equals to the total noise power on the system bandwidth [22]. From Figure 11 b, the SFDR is calculated as

$$SFDR = \frac{2}{3} 10 \log_{10} \left(\frac{IP3}{N_{out} R} \right) \left(dB - Hz^{\frac{2}{3}} \right) \tag{2.24}$$

where R is the system bandwidth

N_{out} is the total noise at the output of the detector

2.5 Implementations of Photonic Filters

This section describes the practical implementations and the operating principles of incoherent photonic filters. The main classification criteria in the implementation of the photonic filters is the number of sources employed in their setups. In one class (Single source microwave photonic filter) only one laser

source (either tunable or at a fixed wavelength) is used to be modulated by the RF signal. This type of filters suffer from the FSR limitations since coherence length of the laser sets a lower limit to the minimum delay applicable for incoherent operation. For multiple source microwave photonic filters (MSMPF) however, different lasers at different wavelengths are utilized for the implementation of delays. There is no FSR limitations in these type of filter since the deterministic relation between the phases of the carriers is totally lost [23]. Also methods of implementing filters with negative coefficients are presented due to the large interest they currently attract.

2.5.1 Single Source Microwave Photonic Filters (SSMPF)

The main advantage of single laser systems over the multiple source systems is their low cost. However in order to obtain a stable response, incoherent techniques should be employed which degrade the performance of the filter. First a large linewidth laser is required to ensure incoherence, thus small linewidth lasers for telecommunication applications cannot be employed [14]. Secondly use of single source introduces PIIN noise to the signal which is the dominant source degrading system performance. A novel method to eliminate the PIIN and the coherence effects is introduced in [14] with the schematic given in Figure 12.

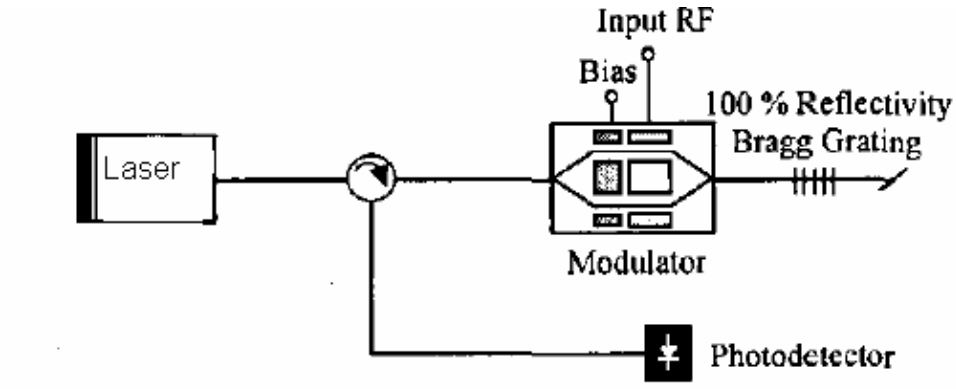

Figure 2.10 A coherence free single source photonic filter

In this structure the optical carrier passing through the isolator is modulated at the modulator in the forward direction. After being reflected back from the Bragg grating the modulated carrier reenters the modulator to experience a second modulation and directed to the photodetector by the circulator. The frequencies at which the signal experiences 180 degrees phase shift are the points where the filter response has the notches. Thus the distance between the modulator and the grating controls the notch frequencies. Interference causing coherence is eliminated since single carrier exists in the system as a result small linewidth source can be employed for this filter.

This filter has another advantage that with the employment of chirped grating instead of uniform Bragg grating the notch frequencies may be tuned by changing the laser wavelength (which requires a tunable laser source).

The schematic of another single source photonic filter that utilizes an active medium to increase the number of taps, which is purposed in [23], is given in Figure 2.11.

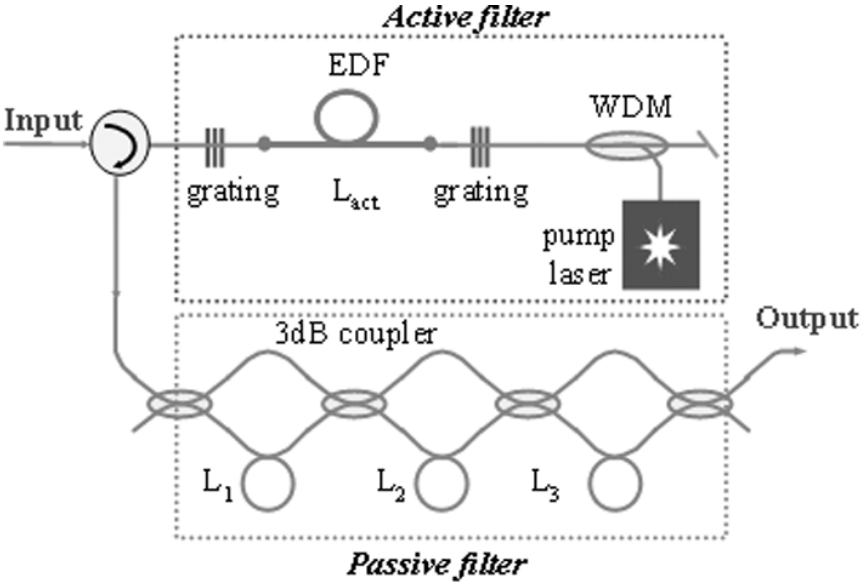

Figure 2.11 A hybrid filter that utilizes an active medium to increase the number of taps

In this structure the first grating (at the left of EDF) has a reflectivity of 50%

whereas the second grating has a reflectivity of 100%. Half of the signal is reflected at the first grating and the other half enters to erbium doped fiber (EDF) to be amplified. The pump laser provides the energy for the amplification process. The amplified signal is reflected back from the second grating and passes again from the amplifying medium. Reaching to the first grating, again same part is reflected back to the amplifying medium and the other part is sent to the detector. Increasing the gain of the amplifying medium, the number of reflections between the cavities of the sample may be increased resulting in increased number of taps. At the point where the gain of the EDF totally compensates for the losses in the system the number of taps is infinity. However this condition is not implemented in practice because of the stability considerations.

Note that in Figure 11 a passive filter is attached to the output of the active section of the filter. This part is used to eliminate the intermediate peaks and to select the multiple that corresponds to the desired frequency [22]. In fact this hybrid filter is one of the highest Q photonic filters with a quality factor around 900 [23].

2.5.2 Multiple Source Microwave Photonic Filters (MSMPF)

As mentioned earlier, the main drawback of SSMPFs is the introduction of PIIN and degrading the SNR performance of the system. Although solutions to overcome this problems are purposed, increasing the number of taps in these structures is rather difficult. MSMPFs on the other hand do not introduce coherence problems and it is easier to construct flexible, reconfigurable and tunable filters using multiple sources.

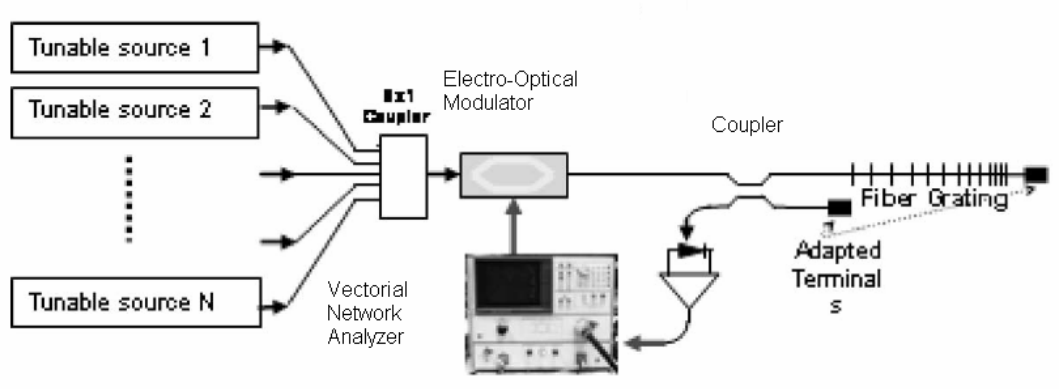

Figure 2.12 A MSMPF based on laser array

In the MSMPF given in Figure 2.12 is purposed in [24]. The structure consists of an array of N lasers and each wavelength experiences different delay at the linearly chirped grating. The amount of delay T can be controlled by changing the wavelengths of the tunable sources. Also if the output powers of the lasers are adjustable apodization can be applied easily to the filter impulse response [8].

Another type of MSMPF that utilizes dispersive medium to implement delay is shown in figure 2.13. The operation principle of this filter depends on the different delays encountered by different wavelengths at the input. These filter offer same advantages as the filter given in figure 2.12 however the dispersive element used is generally long fiber which introduces excessive loss to the system the compensation of which requires extra amplifying components.

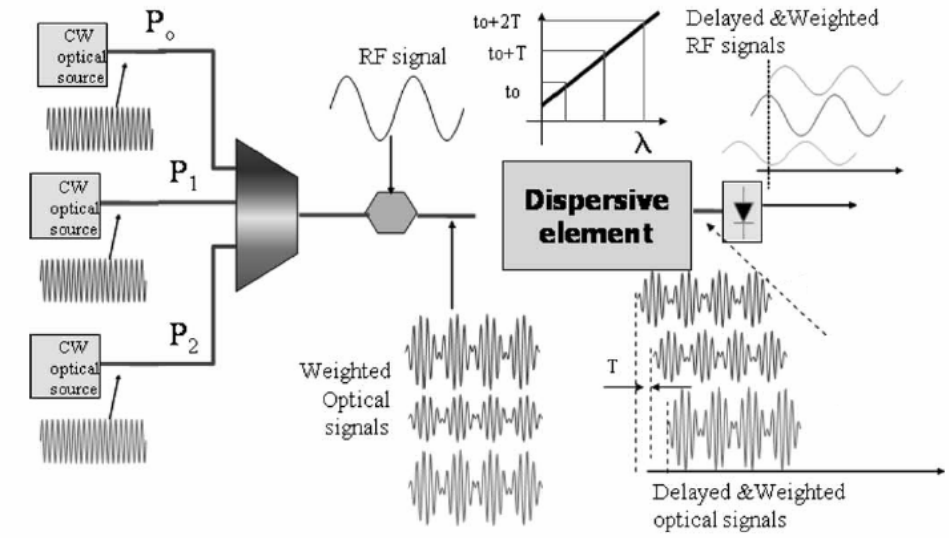

Figure2.13 MSMPF utilizing dispersive medium

2.5.3 Implementation of Negative Taps

It was aforementioned that coherent filters are not implemented in practice because of the sensitivity to environmental conditions such as vibrations and changes in temperature. The incoherent filters are introduced to solve this problem. However use of the incoherent filters introduce another drawback, the positive tap coefficients. The lack of negative coefficients does not allow design of filters with flat bandpass and sharp transitions, also there is always a resonance at baseband [2].

One method to solve this problem is known as the differential detection since it uses two opto-electronic converters with the response of one inverted. The operating principle is shown in Figure 2.14. The impulse response of the filter is divided into two parts one of which is includes positive coefficients and the other contains all negative coefficients. The two sections are implemented using incoherent approach, i.e. with positive coefficients. At the detection stage the optical signal at the positive coefficient side is fed to a noninverting diode whereas the optical signal at the negative coefficient side is fed to an inverting diode to achieve inversion. With this technique every negative coefficient filter can be constructed. However the requirement of extra component for the implementation and the requirement for careful path balance to ensure robust characteristics make this technique less attractive [22].

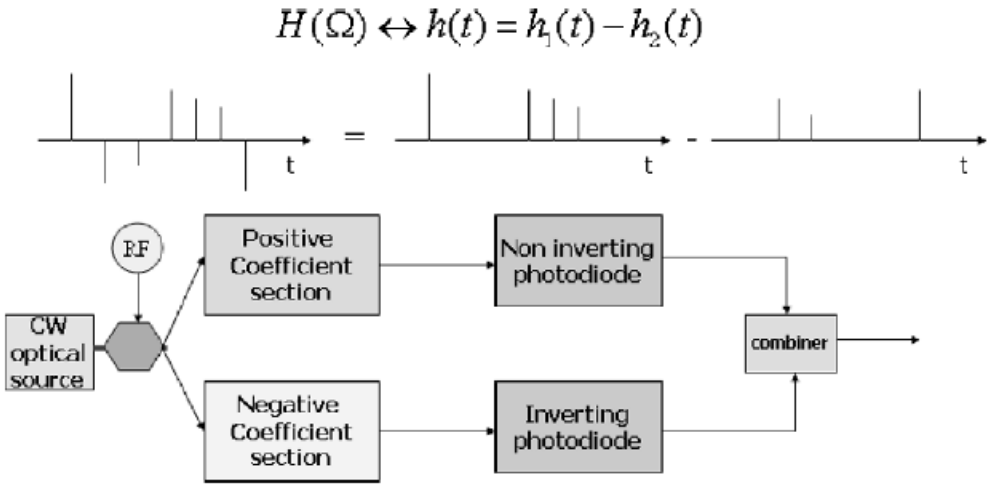

Figure 2.14 Implementation of negative taps using differential detection

2.6 Practically Implemented Filters

2.6.1 The FIR Filter

The following setup is constructed to construct a two tap low pass filter.

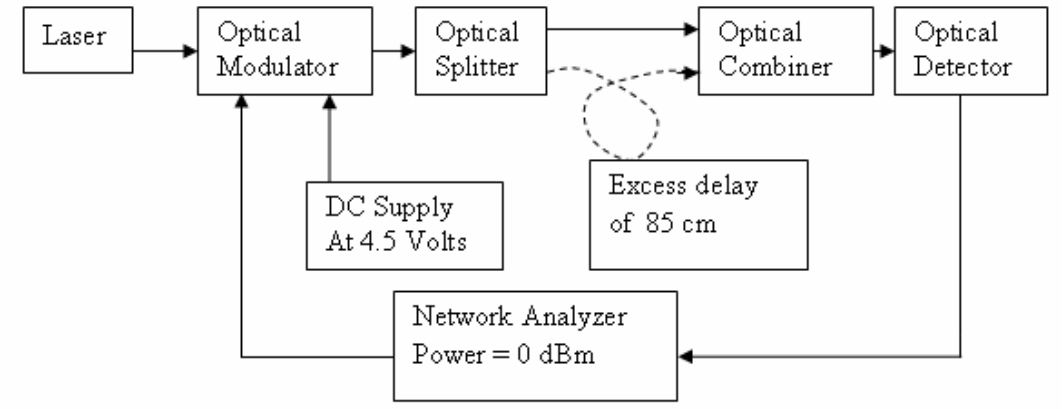

Figure 2.15 The setup of the two tap fir filter

The optical signal from the laser is fed to the optical modulator. The DC bias of the modulator is adjusted to the point where maximum modulation index is achieved. The RF input of the modulator is fed from Port1 of the network analyzer (HP4395A). The modulated carrier at the output of the modulator is

fed to an optical splitter. One arm of the optical output is fed directly to the input of the optical combiner whereas the second arm introduces a delay using a 85 cm fiber. The output of the combiner is fed to the optical detector to achieve electro-optical conversion and the electrical signal is fed to the second port of the network analyzer to observe the frequency response of the system.

Note that the system has a simple transfer function of $H(z)=1+z^{-1}$. The excess delay experienced by the optical signal at the 85 cm fiber is,

$$\tau = \frac{l}{v} = \frac{0{,}85}{2\times 10^{8}} = 4.25\times 10^{-9}$$ where v is the speed of light in fiber

Thus the filter will notch at the frequency where the $4.25*10^{-9}$ seconds delay corresponds to 180 degrees of phase shift i.e.

$$2\pi \times 4.25\times 10^{-9} \times f = \pi \;\Rightarrow\; f = 117.6\,MHz$$

The response obtained is shown in Figure 2.16.

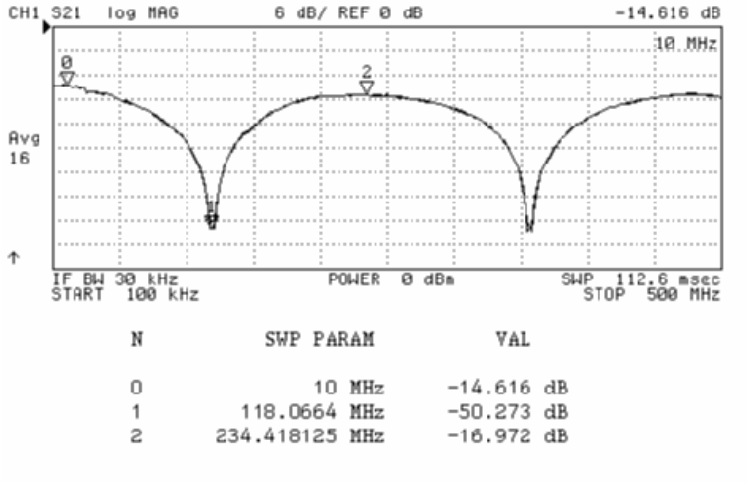

Figure 2.16 the response of fir filter

The noise mechanisms in two-tap filter

In order to analyze the noise behavior of the system following procedures are applied, which are adapted from [11].

First the laser turned off and the second path to the optical combiner was disconnected. This setup measured the noise floor of the system (i.e the noise due to the optical detector)

Secondly the laser is turned on and Relative Intensity Noise (RIN) due to the laser was measured.

Lastly the second path to the optical combiner was connected which allows to measure the Phase Induced Intensity Noise (PIIN) of the system.

In the Figure 2.17 the weakest noise is the detector noise, the curve above the detector noise is the Relative Intensity Noise and the noise that dominates by far is the Phase Induced Intensity Noise.

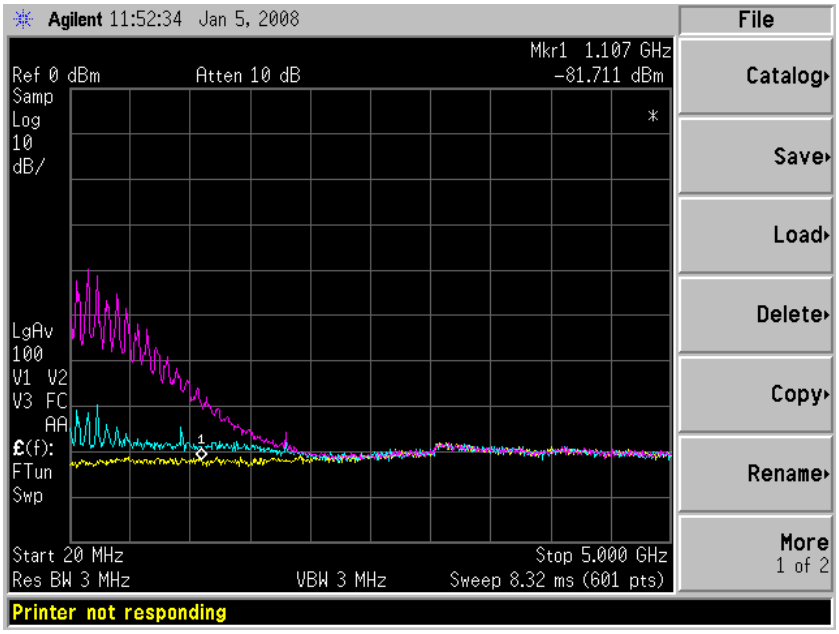

Figure 2.17 Noise contributions in two-tap filter

In the above figure the decrement in PIIN as the frequency is increased is due to the narrow bandwidth of the frequency response of the detector and the fluctuations are due to the back reflections within the circuit.

2.6.2 The IIR Filter

In order to implement an IIR filter the setup shown in figure 2.18 is constructed.

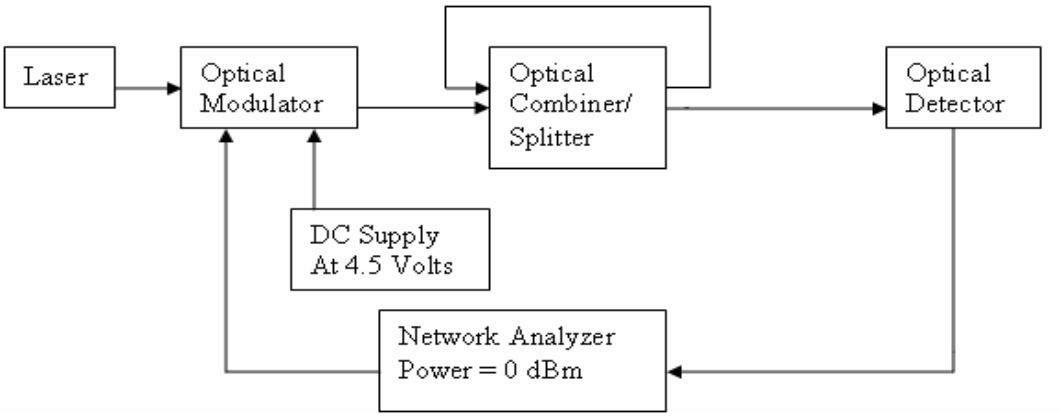

Figure 2.18 The schematic of the IIR filter

The delay in this filter is introduced in the feedback path at the optical combiner/splitter. The transfer function of the filter can be derived by tracing the optical signal at the splitter.

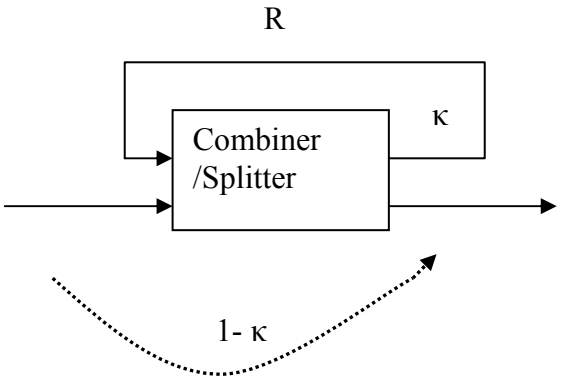

Figure 2.19 the coupling at the combiner/splitter

The first tap is the signal that encounters no delay in the splitter and has the coefficient 1- κ.

For the second tap, the signal passes to the upper arm of the splitter and fed back to the input of the combiner. The delay encountered is the length of the feedback path. Assuming the loss in the feedback path is R, the magnitude of the second tap is $\kappa^2 R$

For the third tap the signal makes two rotations in the loop which leads to a tap coefficient of $\kappa^2 R^2(1-\kappa)$.

Continuing that way the overall transfer function of the filter is given by the sum

$$H(z) = (1-\kappa) + \kappa^2 \sum_{n=1}^{\infty} (1-\kappa)^{n-1} R^n z^{-n} \tag{2.25}$$

For the filter constructed in the setup which is given in Figure 2.18, the coupling coefficient is 0.7. The response observed at the Network analyzer and the results of the simulation of the transfer function in matlab is given in Figure 2.20 a) and b) respectively.

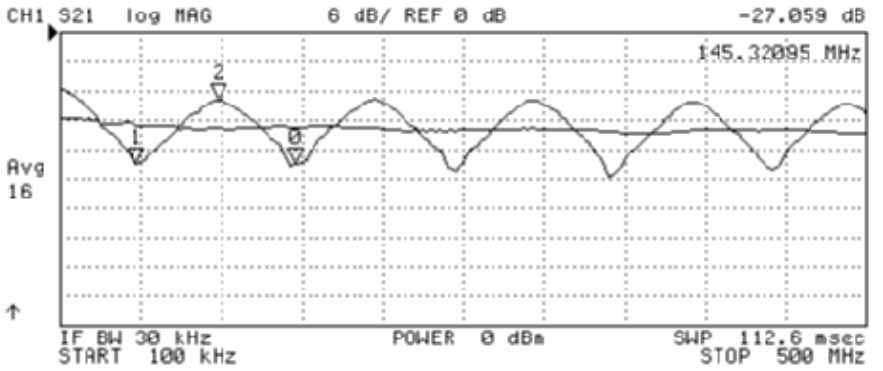

N	SWP PARAM	VAL
0	145.32095 MHz	-27.059 dB
1	46.5907 MHz	-26.908 dB
2	97.705475 MHz	-13.689 dB

(a) the plot taken from network analyzer

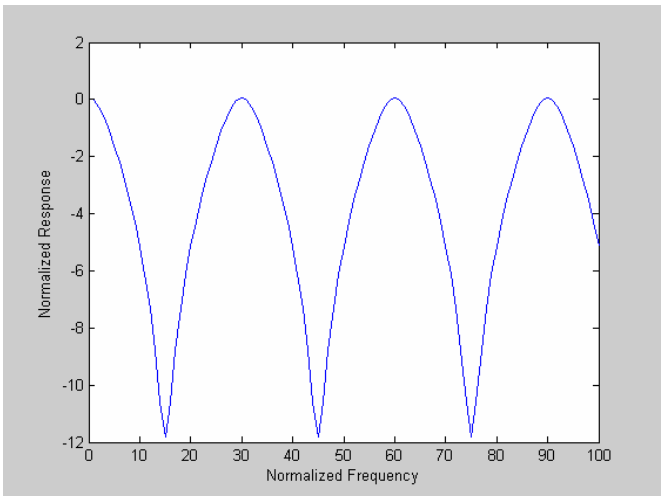

b) simulated response in matlab

Figure 2.20 the response of the IIR filter a) the plot taken from network analyzer b) simulated response in matlab

In this type of IIR filters the sharpness of the filter can be adjusted by changing the coupling coefficient κ, of the coupler. The sharpest response is obtained at κ = 0.33 which is purposed in [1]. A matlab simulation with κ = 0.33 gives the filter response as in figure 2.21.

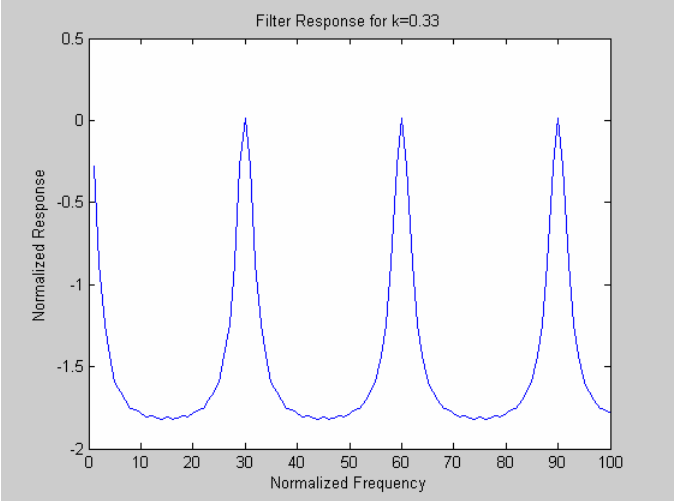

Figure 2.21 Filter Response for κ = 0.33

CHAPTER 3

THE PHOTODETECTOR and THE LASER

3.1 The Photodetector

The task of an optical detector is to convert optical energy to electrical energy using photoelectric effect [25]. A photodetector should achieve this task without adding noise to the signal and without distorting it. Also the detector should not waste any input power and have a fast response to detect optical signals modulated at high rates.

The figures of merit of the photodetectors are the quantum efficiency, responsivity, bandwidth, noise equivalent power (NEP) and spectral response each of which will be discussed next

3.1.1 The Quantum Efficiency

The principle of operation of a photodetector is creation of electrical charges by the absorption of optical energy, namely photons. The quantum efficiency is the parameter showing how efficient the detector converts photons into electrical carriers. It is denoted by η and is given by

$$\eta = \frac{number\ of\ electrical\ carriers\ created}{number\ of\ incident\ photons}$$

Quantum efficiency determines the signal to shot noise ratio, thus the SNR of the detector at high optical intensities. Given the absorption rate "α" of the detecting medium of length L, the transmitted power through the medium is $P_{out}=P_{in}*\exp(-$

αL) and the absorbed power is $P_{abs}=P_{in}(1- \exp(-\alpha L))$. Since each absorbed photon creates an electron-hole pair [25],

$$\eta = \frac{P_{abs}}{P_{inc}} = 1 - e^{-\alpha L} \tag{3.1}$$

3.1.2 The Responsivity

The responsivity is the ratio of the output current of the detector to the incident power in the units of amperes per watt. The responsivity ($\Re$) can be expressed in terms of quantum efficiency as

$$\Re = \frac{\eta q}{h\nu} \approx \frac{\eta \lambda}{1{,}24} \tag{3.2}$$

Note that the responsivity of a detector increases as the wavelength of the optical signal increases. This is due to the increased number of photons in a given power when the wavelength is increased (the energy of single photon is decreased). However for higher wavelengths the responsivity of semiconductor detectors experiences a sharp decrease since the photon energy falls below the bandgap energy E_g. This is shown in Figure 3.1.

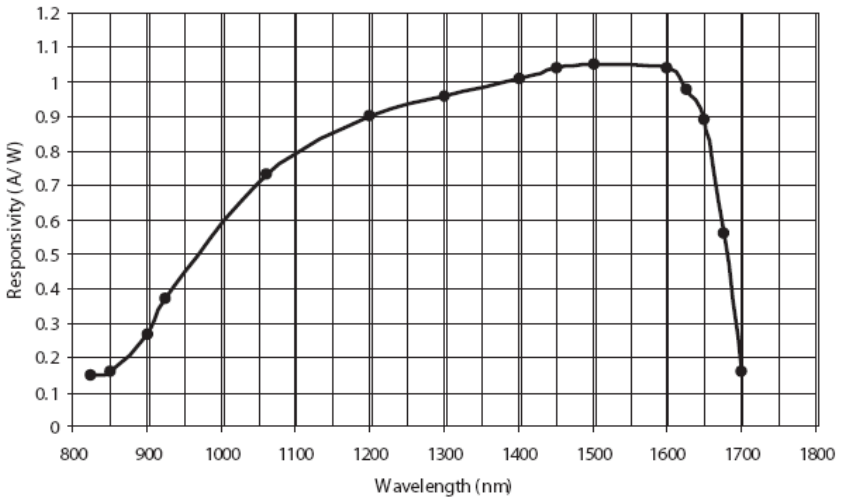

Figure 3.1 Responsivity curve of a semiconductor optical detector

3.1.3 Bandwidth and Capacitance

The bandwidth of a detector determines how fast it responds to the variations of optical power. Two factors influence the bandwidth of the photodetector. One is the RC time constant produced by the capacitance of the detector and the load resistance, the other is the time the carriers require to reach the electrical contact points of the detector.

The time required for the output of the detector to reach from its minimum value to 90% its maximum value is $In(9)RC = 2.2\tau_{RC}$, adding the transit time of the carriers the rise time becomes $T_r = 2.2(\tau_{RC+}\tau_{tr})$ which sets an upper limit to the bandwidth of the detector [25].

3.1.4 The Noise Equivalent Power

Even if no signal is applied to the input of the detector, one still gets output current from the detector. The main reason for that is the thermally generated carriers resulting in so called dark current. One way of representing the noise term at the output of the detector is noise equivalent power (NEP), which is the power level of the incident light to achieve an SNR of 1 at the detector.

The power spectral density of the noise is broadband but not flat, thus NEP is given at a given wavelength and modulation frequency with units watts/√Hz. In order to be able to compare the performance of detectors of different sizes, the NEP is sometimes normalized to a detector area of 1 cm^2 and then is given in units of watts/√Hz/√cm [25].

3.1.5 Spectral Response

The responsivity and the quantum efficiency depend on the absorption coefficient of the material through which the incident optical power propagates. The

absorption coefficient however is a function of wavelength and different substrates are used to detect optical signals at different wavelengths. The most common materials used in communication equipments and the wavelengths at which they are sensitive is given in Table 3.1

Table 3.1 Semiconductor materials and respective wavelength ranges

Material	Bandgap, eV	Wavelength range (nm)	Wavelength of peak response (nm)	Responsivity (max) (A/W)
Si	1.17	300–1100	800	0.5
Ge	0.775	500–1800	1550	0.7
InGaAs	0.75–1.24	1000–1700	1700	1.1

3.2 The PIN Diode

The structure of the pin diode is given in Figure 3.2 where the intrinsic region is sandwiched between the p and the n regions. The photons arriving to the detector pass through an antireflection coating which prevents the striking photons to be reflected back from the surface of the detector [6]. The photons also pass through the thin, highly doped p-region and enter the intrinsic region. Intrinsic region is the place where the photons are absorbed and electron-hole pairs created. Longer regions increase the probability of absorption however they also make the path of free electrons and holes longer, which increase the amount of time required to reach contact points. Thus diodes with longer intrinsic regions are more sensitive but slower than those with shorter intrinsic regions.

Under the influence of external electric field the free electrons and holes reach the contact points and create an external current flow which is then detected by the external electronic circuitry.

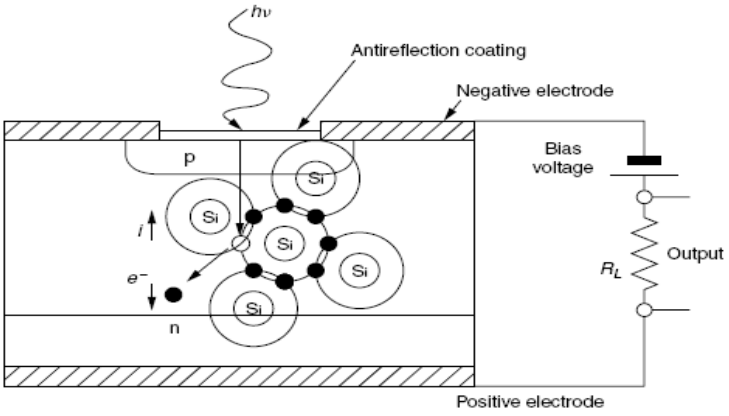

Figure 3.2 The Structure of a PIN diode

3.3 The Laser

A laser consists of three components, an active region with energy levels that can be selectively populated, a pump to produce population inversion between the energy levels and an electromagnetic cavity which contain the active medium and provides feedback to create oscillations.

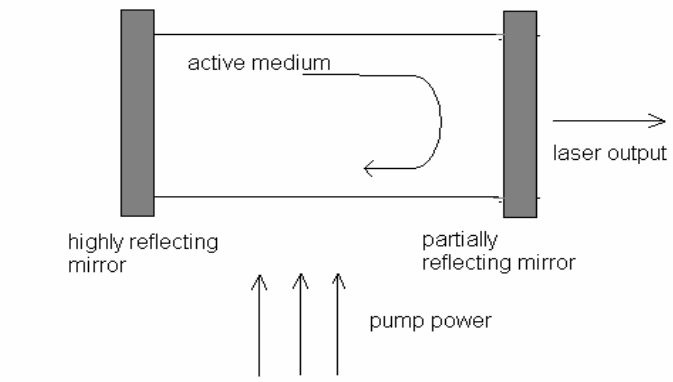

Figure 3.4 Laser Structure

Quantum theory shows us that matter exists only in certain allowed energy levels. In thermal equilibrium lower energy states are more likely occupied than the higher energy states. If a photon with energy equal to the energy difference between the states hits an atom at lower energy the atom absorbs the photon and

is excited to the upper state. This is known as absorption. Inversely if the atom hits an excited atom, a second photon with same polarization and energy is created leaving the atom in lower energy state. This process is known as the stimulated emission and constructs the basis of lasing.

For a two level system in thermal equilibrium Boltzman distribution law dictates that the number of atoms in the excited state to be less than the number of atoms in lower state. However in order to provide a stimulated emission rate greater than the absorption rate, the number of excited atoms should be larger than the photons in ground state, which is known as population inversion.

However two level systems are not suitable for population inversion hence three or four levels systems are utilized in practice. The operation of a three level system is described below.

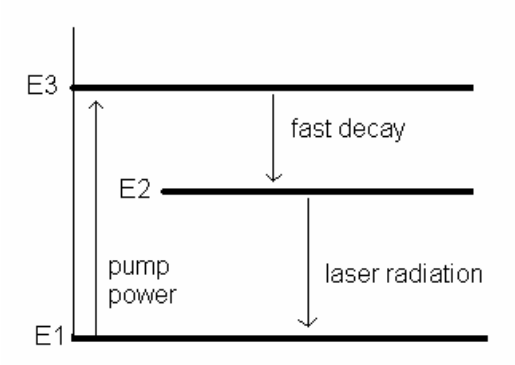

Figure 3.5 Three Level Laser System

- Atoms in the lowest energy state E1 are excited to E3 by the pumping process which requires an external source

- Since E3 is an unstable energy level, electrons decay to E2 rapidly. The energy is lost as lattice vibrations (phonons). Electrons stay in E2 for longer time since E2 is a metastable energy state. If the electrons in E1 are excited at a faster rate to E3 than the decay rate from E2 to E3, population inversion is achieved between E2 and E1. As a result photons with energy E2-E1 can

create new photons with same energy utilizing stimulated emission process[5].

The energy levels in figure 3.5 are plotted as solid lines which result in single oscillation frequency. In practice however the energy levels are not solid lines rather they form energy bands. This results in wider spectrum of laser output called as linewidth.

Once the gain in the active medium is large enough to compensate for the losses in the cavity (losses in the mirrors and absorption losses) then the amplitude of the oscillations increase up to value where saturation effects start to become effective. Since the photons create standing waves in the cavity only certain frequencies could exist within the cavity. The discrete frequencies are given by the formula:

$$f = m * \frac{c}{2nL} \tag{3.3}$$

where f is the frequency of oscillation

c/n is the speed of light in the cavity

L is the length of the cavity

m is an integer

this condition along with the linewitdh of the active medium result in the spectra whose shape is given in figure 3.6 which is in fact the laser we utilized in this thesis.

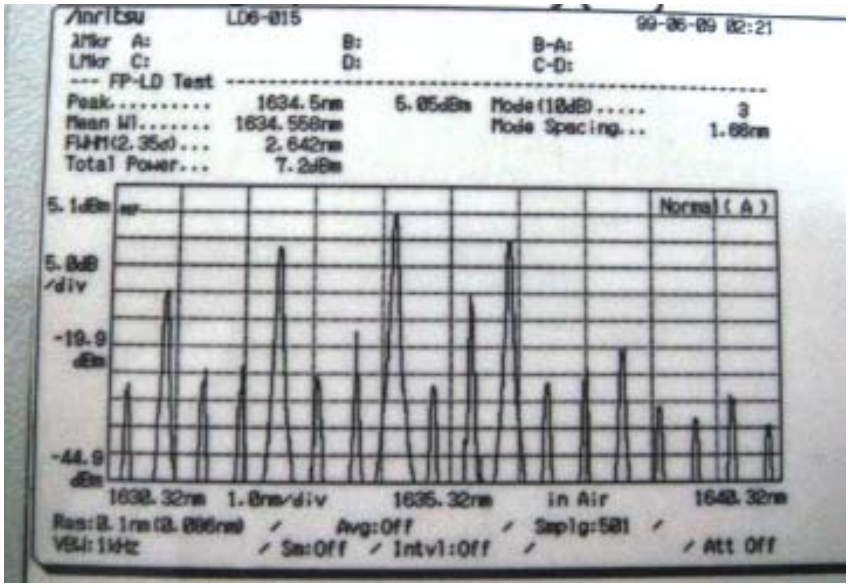

Figure 3.6 The Spectrum of Laser Output

CHAPTER 4

HARMONIC GENERATION USING LiNbO3 OPTICAL MODULATOR

4.1 The Theory of Operation

Optical modulators are devices that alter the phase and/or amplitude of the optical carrier when an external electric field is applied. Many different mechanisms are utilized in order to achieve optical modulation. The major mechanisms used are,

- Electro-optic Modulation
- Acousto-optic Modulation
- Magneto-optic Modulation
- Mechanical and Micromechanical Modulation [27]

The modulator used in this thesis is an electro-optical modulator and only the operating principle of these type modulators will be presented here.

Electro-optic modulators utilize the change in the index of refraction of certain types of crystals when an external field is applied. This linear electro-optic effect is also known as Pockels effect named after F. Pockel who studied the effect in 1983 [28]. The underlying theory will be briefly introduced here, for detailed analysis one may refer to [27] [28] [29].

In an anisotropic media the displacement vector $\bar{D}$ and the electric field $\bar{E}$ are related by $\bar{D} = \bar{\varepsilon} \bullet \bar{E}$, where $\bar{\varepsilon}$ is the permittivity tensor. For nonmagnetic materials the permittivity tensor is real and symmetric which means that by proper selection of coordinate axes one may obtain a diagonal $\bar{\varepsilon}$ as

$$\bar{\varepsilon} = \begin{bmatrix} \varepsilon_x & 0 & 0 \\ 0 & \varepsilon_y & 0 \\ 0 & 0 & \varepsilon_z \end{bmatrix} = \varepsilon_0 \begin{bmatrix} n_x^2 & 0 & 0 \\ 0 & n_y^2 & 0 \\ 0 & 0 & n_z^2 \end{bmatrix} \tag{4.1}$$

Where n_i are the principle indices of refraction and the matrix on the right is called as the optical dielectric tensor. Then the phase velocity of an optical beam polarized in i^{th} direction is c/n_i .

The optical dielectric tensor depends on the charge distribution within the crystal. Thus the application of an external electric field may change the charge distribution and thereby the optical dielectric tensor. This is known as the electro-optic effect.

Conventionally the change in the optical dielectric tensor due to external electric filed is given by the equation

$$\Delta\eta_{ij} = \Delta\left(\frac{1}{n^2}\right)_{ij} = \sum_{k=1}^{3} r_{ijk} * E_k \tag{4.2}$$

where k is the direction of the applied electric field and r_{ijk}'s are the experimentally determined linear electro-optic coefficients.

The modulator used in the thesis utilizes $LiNbO_3$ crystal which is a uniaxial crystal with impermeability tensor,

$$\begin{bmatrix} 1/n_o^2 & 0 & 0 \\ 0 & 1/n_o^2 & 0 \\ 0 & 0 & 1/n_e^2 \end{bmatrix}$$

with n_0=2,29 and n_e=2,20

The electro-optic coefficients of the $LiNbO_3$ crystal are given as

$r_{113}=r_{223}$	$=8,6$	10^{-12} m/V	
$r_{222}= -r_{112}= -r_{122}= -r_{212}$	$=3,4$	10^{-12} m/V	
r_{333}	$=30,8$	10^{-12} m/V	
$r_{232} =r_{322} =r_{131} =r_{311}$	$=28$	10^{-12} m/V	[28]

Since r_{333} is the largest among the electro-optic coefficients it can be utilized for the maximum change in the index of refraction foe a given electric field E.

Consider the structure given in Figure 4.1 where the wave is polarized in z direction and propagates in x direction. If the external field is applied in z direction the change in impermeability tensor would be,

$$\Delta\left(\frac{1}{n^2}\right)_{33} = r_{333} * E_z \tag{4.3}$$

and

$$\Delta\left(\frac{1}{n^2}\right)_{11} = \Delta\left(\frac{1}{n^2}\right)_{22} = r_{223} * E_z \tag{4.4}$$

from the formula 4.2

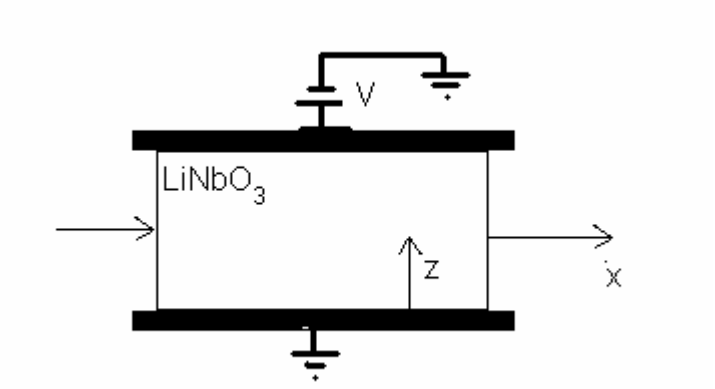

Figure 4.1 The direction of the applied filed and polarization

Thus the uniaxial property of the crystal does not change due to the external electric field. The change in the refractive index in z direction can be found by the assumption $r_{333*}E<<1/n^2_e$ use of the differential formula $dn = -\left(n^3/2\right)* d\left(1/n^2\right)$

which gives

$$n_z = n_e - \frac{n_e^3}{2} * r_{333} * E_z \tag{4.5}$$

The phase shift relative to the case in which no field is present can be calculated once the change in the refractive index is known. It is given by the equation

$$\Delta\phi = \frac{2\pi}{\lambda}\left[-\frac{1}{2} * n_e^3 * r_{333} * \left(\frac{V}{d}\right) l\right] \tag{4.6}$$

Where V/d is substituted for the applied electric field and l is the length of the crystal.

The half wave voltage V_π is defined as the voltage at which the applied field a phase shift of π and is given by

$$V_\pi = \frac{\lambda}{n_e^3 * r_{333}} \frac{d}{l} \tag{4.7}$$

4.2 The Structure of Mach-Zender Modulator

In optical communications most electro-optic modulators utilize Mach-Zender structure whose structure is given in Figure 4.2

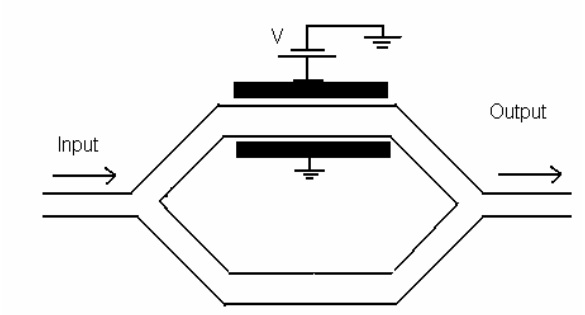

Figure 4.2 The structure of Mach-Zender Modulator

The optical signal is split into two arms and external voltage is applied to one of the arms to introduce relative phase shift. Finally the signals at to arms are combined to yield output. The output intensity is given by

$$I_{out} = \left| \frac{1}{\sqrt{2}} E e^{-j\phi_1} + \frac{1}{\sqrt{2}} E e^{-j\phi_2} \right|^2 = \frac{1}{2}(1+\cos\Delta\phi) I_{in} \quad (4.8)$$

Where E is the electric field of the optical carrier and should not be confused with the external electric field due to the applied voltage to the electrodes. Also $\Delta\phi$ is the relative phase shift between two arms. As is obvious from the formula an applied voltage changes $\Delta\phi$ and thereby the amplitude of the optical carrier thus amplitude modulation is achieved using mach-zender structure.

4.3 Generation of Harmonics

In order to generate harmonics of a signal, nonlinear property of the optical modulator is utilized. The transfer function relating the modulators output light intensity to the applied bias voltage is given by the formula

$$I_{output}(V) == I_{input} * \frac{1}{2}\left(1+\cos\left(\pi \frac{V}{V_\pi}\right)\right) \quad (4.9)$$

Where

V = Applied Voltage to the Modulator

V_π= The voltage range which changes the output from maximum to minimum

The modulator's characteristics curve is plotted below in Figure 4.3

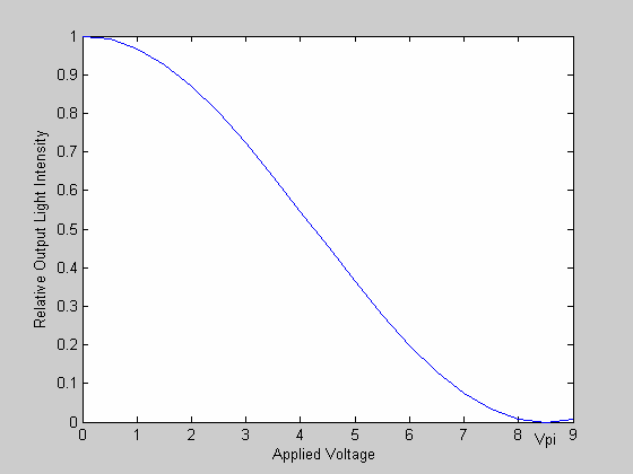

Figure 4.3 The response of modulator

The input voltage to the modulator consists of a DC term, which determines the quiescent point and an AC term as the modulation signal. So, the input voltage to the modulator can be expressed as

$$V_{in} = V_{DC} + \left(V_1 \sin\left(\omega_1 t\right) + V_2 \sin\left(\omega_2 t\right)\right) \qquad (4.10)$$

Putting the input voltage value in (2) into (1) one gets the output intensity function as

$$\mathrm{I_{output}} = \frac{1}{2}\mathrm{I_{input}} * \Bigg(1 + \left[\cos\left(\pi \frac{\mathrm{V_{DC}}}{\mathrm{V_\pi}} \right) \times \cos\left(\mathrm{V_1 sin(\omega_1 t) + V_2 sin(\omega_2 t)}\right) \right] - \left[\sin\left(\pi \frac{\mathrm{V_{DC}}}{\mathrm{V_\pi}} \right) \times \sin\left(\mathrm{V_1 sin(\omega_1 t) + V_2 sin(\omega_2 t)}\right) \right] \Bigg) \qquad (4.11)$$

Using the identities

$$\sin(x + y) = \sin x \,.\, \cos y + \cos x \,.\, \sin y$$

$$\cos(x + y) = \cos x \,.\, \cos y - \sin x \,.\, \sin y,$$

$$\cos(x \,.\, \sin\theta) = J_0(x) + 2\, J_{2n}(\mathrm{x}) * \sum_{n=1}^{\infty} \cos 2n\theta,$$

$$\sin(x \,.\, \sin\theta) = 2^{*}\sum_{n=1}^{\infty} \quad J_{2n-1}(x)^{*}\sin(2n-1)\theta$$

the output intensities is obtained as

$$I_{output} = \frac{1}{2} I_0 \left(1 - \cos\left(\pi \frac{V_{DC}}{V_\pi} \right) J_0\left(\pi \frac{V_1}{V_\pi} \right) J_0\left(\pi \frac{V_2}{V_\pi} \right) \right)$$

$$+ 2\cos\left(\pi \frac{V_{DC}}{V_\pi} \right) \sum_{\alpha_k} \left(\prod_{k=1}^{2} J_{|\alpha_k|}\left(\pi \frac{V_k}{V_\pi} \right) \cos\left(\sum_{k=1}^{2} \alpha_k \omega_k t \right) \right) \qquad (4.12)$$

$$+ 2\sin\left(\pi \frac{V_{DC}}{V_\pi} \right) \sum_{\gamma_k} \left(\prod_{k=1}^{2} J_{|\gamma_k|}\left(\pi \frac{V_k}{V_\pi} \right) \sin\left(\sum_{k=1}^{2} \gamma_k \omega_k t \right) \right)$$

for

$$\sum_{k=1}^{2} |\alpha_k| = \text{even integer only}$$

$$\sum_{k=1}^{2} |\gamma_k| = \text{odd integer only}$$

4.4 PRACTICAL SETUP

In order to generate harmonics of a signal the setup shown in Figure 4.4 is constructed

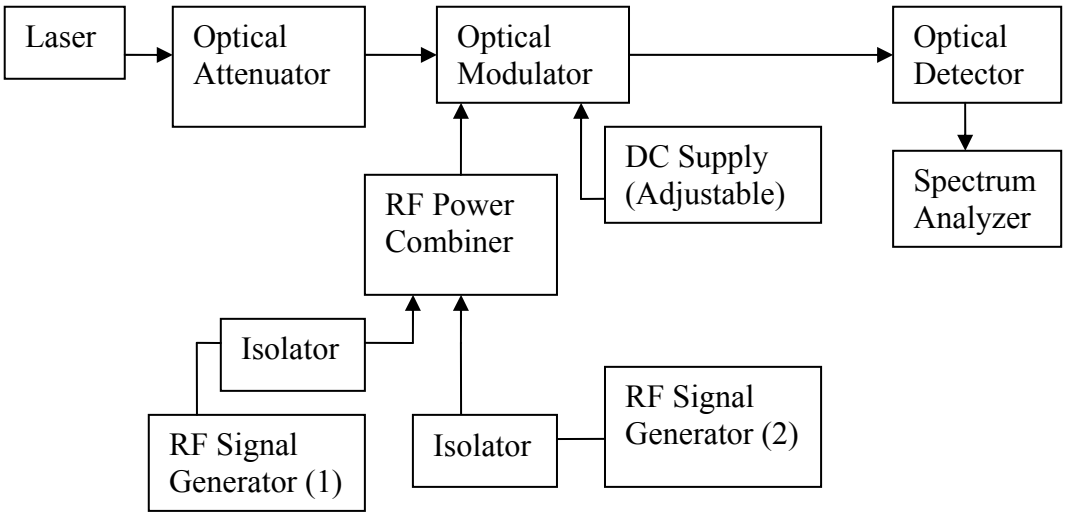

Figure 4.4 Setup to create and analyze harmonics

To generate harmonics the quiescent point of the optical modulator is changed by adjusting the DC power supply at the DC input of the modulator.

At the RF port of the modulator two signal generators are combined to allow two tone modulation.

Optical attenuator and the isolators are inserted in order to be sure about the linearity of the RF signal generators and the optical detector. When generators and the detector also show nonlinear behavior then it may be difficult to analyze the nonlinearity which is caused only by the modulator.

4.4.1 The Linearity of The Generators

The signal generators used in de setup are the Agilent's 8657A and E4434B model signal generators. At high output levels (higher than 5 dBm) harmonics of the fundamental signal is observed at the output of the generators. Also some intermodulation products are observed due to the interaction between the generators. In order to reduce the amplitudes of the spurious frequencies isolators are inserted to the circuit.

The response of one of the isolators is shown below (S21 and S12 curves)

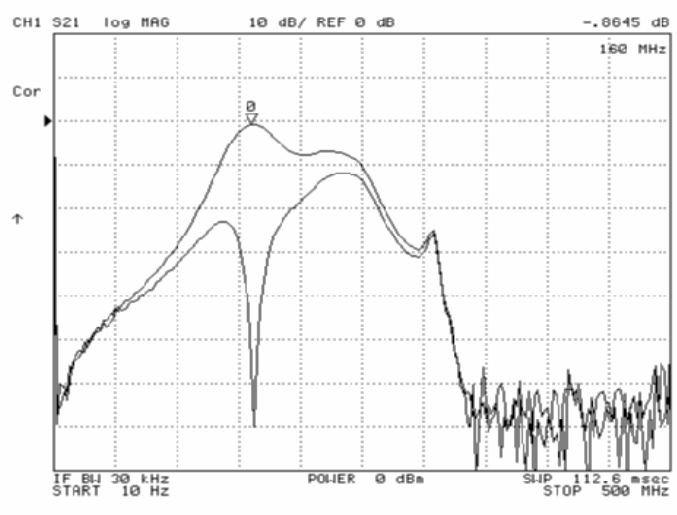

Figure 4.5 the response of isolator

Below two figures show the combined output of the generators before and the after the insertion of the isolators.

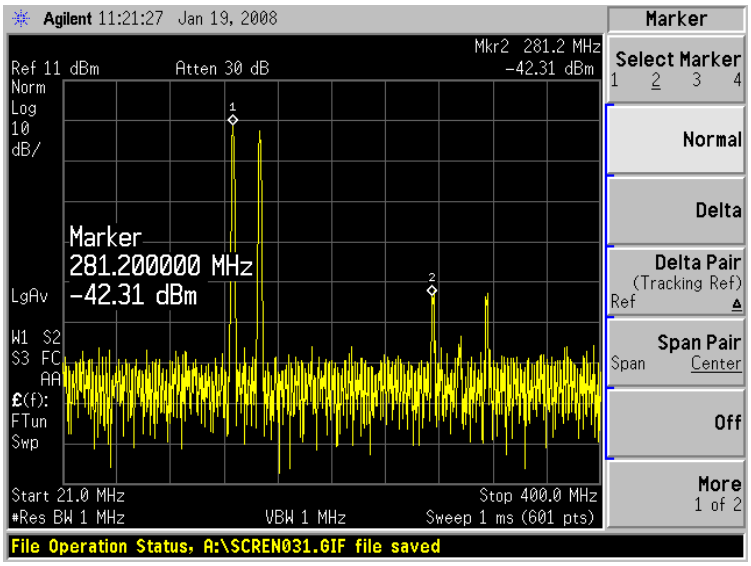

a) Before the insertion of isolators

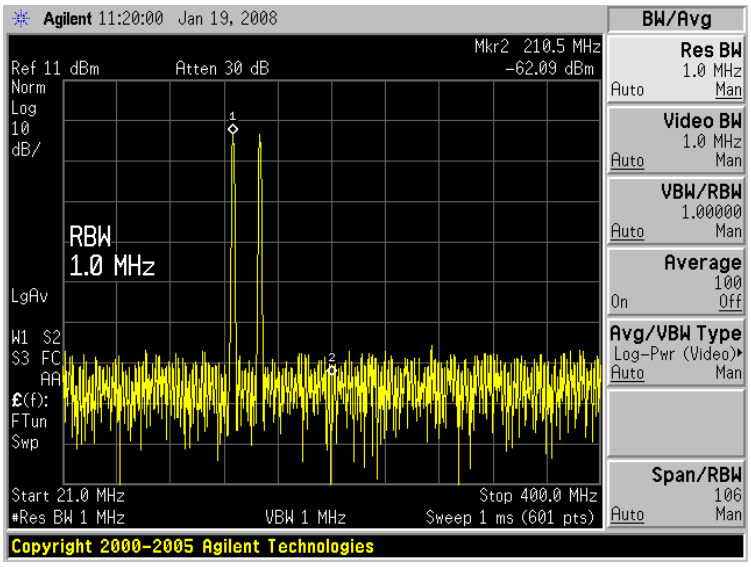

b) After the insertion of isolators

Figure 4.6 the output of the combiner before and after the insertion of isolators

4.4.2 The Linearity of the Optical Detector

Another block that can introduce linearity to the system is the optical detector. The detector used in the setup is Hewlett Packard's PDC2201-2.4. Unfortunately the datasheet of the detector was not available and the optical power level at which the detector starts to become nonlinear was unknown.

To analyze the nonlinearity of the optical detector, the attenuation of the optical attenuator is varied and the change at the output of the detector is observed. For every dB attenuation in the optical attenuator some decrement in the levels at the output of the detector is obtained. The decrement in the detector depends on many factors such as the responsitivity of the detector, optical losses in the system etc.

If the detector is linear then an increment in the optical loss will cause same amount of decrease at all the harmonics.

When the detector does not operate in linear region and harmonics are generated

due to the detector then, if a change in the optical loss causes a decrement of x in the fundamental term, the second harmonic will be reduced by 2x and the third harmonic will be reduced by 3x.

To make the detector to operate in its linear region, optical attenuation is increased to a value where all the harmonics have same differential decrement for some increment in the optical loss.

4.5 Single Tone Modulation

For the analysis of the harmonic terms for the case in which the RF signal applied to the modulator consists of a single tone, the combiner in Figure 4.4 is removed and the signal is applied to the modulator through the isolator.

The amplitudes of the harmonics can be calculated using the formula given in the previous section. The powers of the fundamental and harmonics are proportional to the squares of the given formulas.

The fundamental harmonic has amplitude

$$I_{fund} = 2I_{input} \times J_1\left(\pi \frac{V_1}{V_\pi}\right)\sin\left(\pi \frac{V_{DC}}{V_\pi}\right) \tag{4.13}$$

And the power of the fundamental component is

$$P_{fund}(dBm) = C_1 + 20\log_{10}\left(J_1\left(\pi \frac{V_1}{V_\pi}\right)\sin\left(\pi \frac{V_{DC}}{V_\pi}\right)\right) \tag{4.14}$$

Where C_1 is a proportionality constant concerning the fundamental term

The second harmonic has the power

$$P_{second}(dBm) = C_1 + 20\log_{10}\left(J_2\left(\pi\frac{V_1}{V_\pi}\right)\cos\left(\pi\frac{V_{DC}}{V_\pi}\right)\right) \qquad (4.15)$$

And the third has the power

$$P_{third}(dBm) = C_1 + 20\log_{10}\left(J_3\left(\pi\frac{V_1}{V_\pi}\right)\sin\left(\pi\frac{V_{DC}}{V_\pi}\right)\right) \qquad (4.16)$$

A simulation setup is constructed in the ADS to analyze the signal powers. Although the analytical expressions relating the power levels of the system is given, ADS is utilized since it can plot the spectrum of the output signal and provides some visual help.

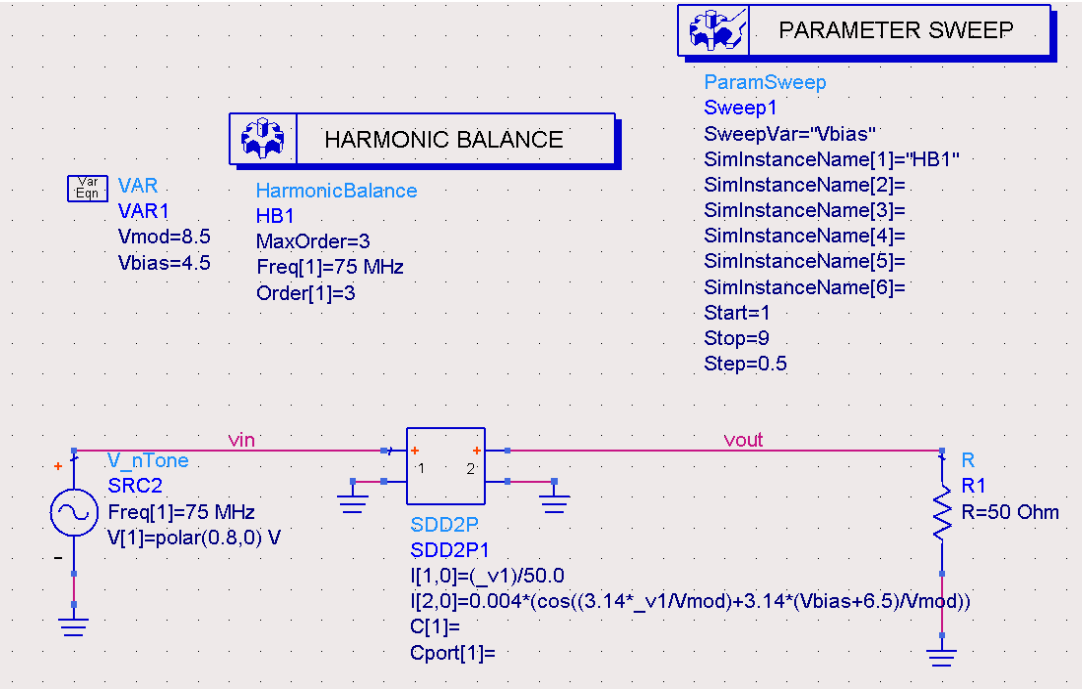

Figure 4.7 Simulation setup to analyze the system

In the simulation, the output current (I[2,0]) of the non-linear two-port is a function (which is the transfer function of the optical modulator) of input

voltage. The amplitude of the voltage applied to the modulator (vin in the simulation) is calculated as follows,

While taking data from the setup, the signal generator supplying input voltage to the optical modulator was adjusted to 75 MHz and 10 dBm.

Reducing the losses in the cables and isolator (about 2,5 dB), the input power at the isolator's RF port is 7.5 dBm. So the input power is;

$$10^{\frac{7,5}{10}} = 5.6\,\text{mW}$$

Since the input impedance of the isolator is 50 ohms, the voltage at the input is

$$\frac{V_{rms}^{\ 2}}{50} = 0,0056 \Rightarrow V_{rms} = 0,529\,\text{V}$$

An the corresponding peak value is 0,529*1.414=0,75V; the value in ADS that fits best to practical data is found to be 0,8 V,

4.5.1 The Fundamental Term:

For the fundamental term the results of the simulation, along with the data taken from the setup and calculation of the formula is given in Figure 4.8

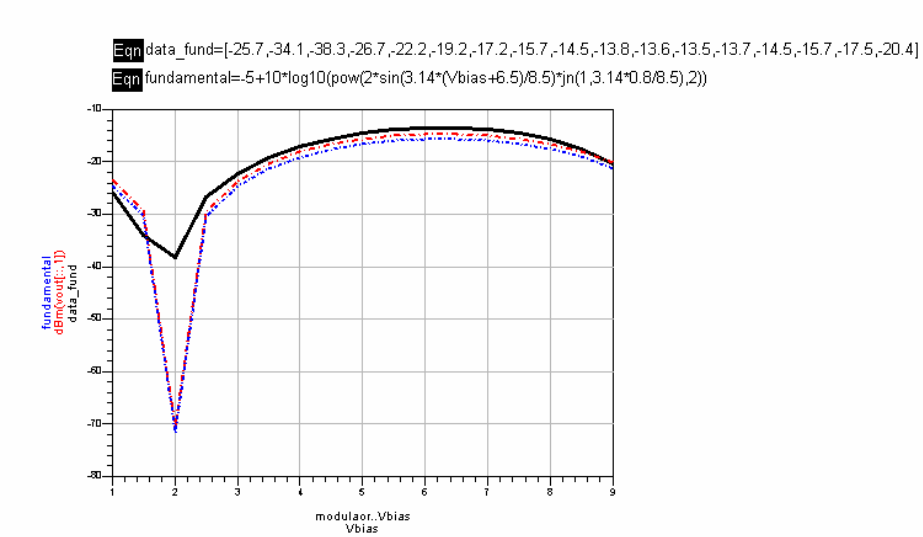

Figure 4.8 Fundamental term versus DC Bias

In the figure the solid line shows data taken from setup, the dashed line shows the calculated response using the formula and the dot-dash line is the ADS simulation result.

4.5.2 The Second Harmonic:

For the second harmonic the results of the simulation, along with the data taken from the setup and calculation of the formula is given in Figure 4.9

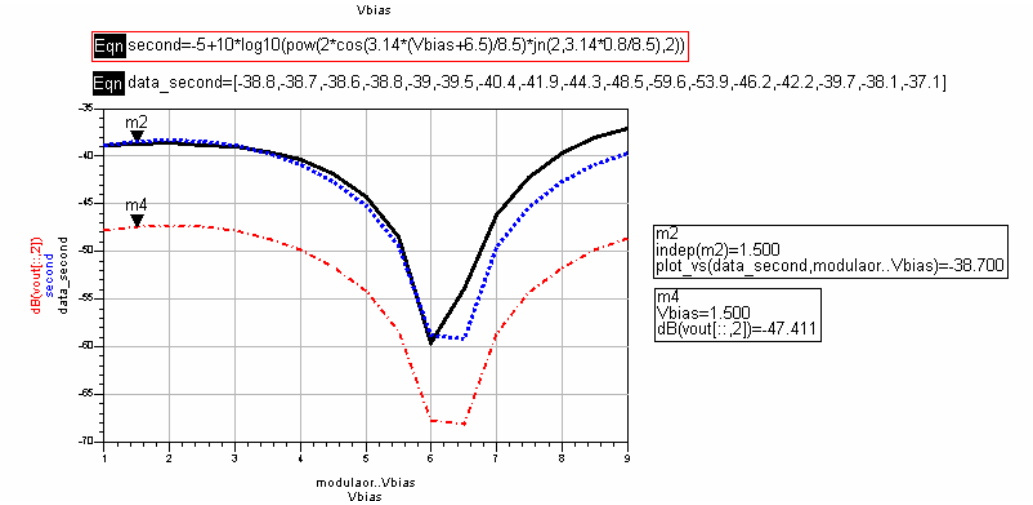

Figure 4.9 Second harmonic versus DC Bias

Note that the dash-dotted line (ADS plot) is about 10 dB lower than the curve obtained using the formula and the data curve. This is because ADS plots the graph relative to 10 dBm.

4.5.3 The Third Harmonic:

For the third harmonic the results of the simulation, along with the data taken from the setup and calculation of the formula is given in Figure 4.10

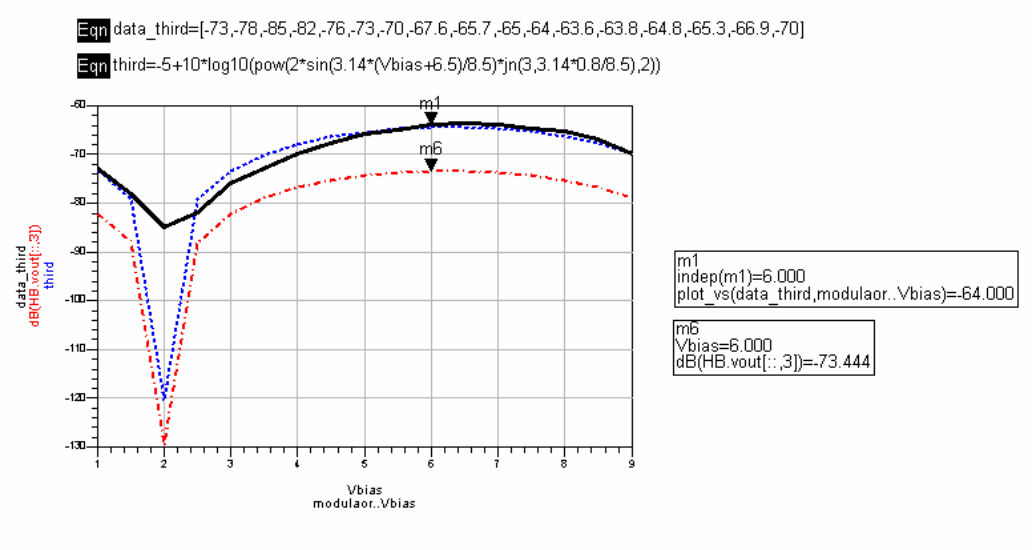

Figure 4.10 Third harmonic versus DC Bias

4.5.4 The Behavior at a Different Signal Level

When the input signal is increased by 5 dB the power levels of the harmonics is observed. It is observed that the fundamental term is increased about 5 dB both theoretically and practically, the second harmonic is increased about 10 dB, and the third harmonic is increased about 15 dB.

The plots are shown in Figure 4.11 a), b) and c)given below, the solid lines correspond to the taken for 10 dBm input and the dot-dashed line correspond to the data taken for 15 dBm input.

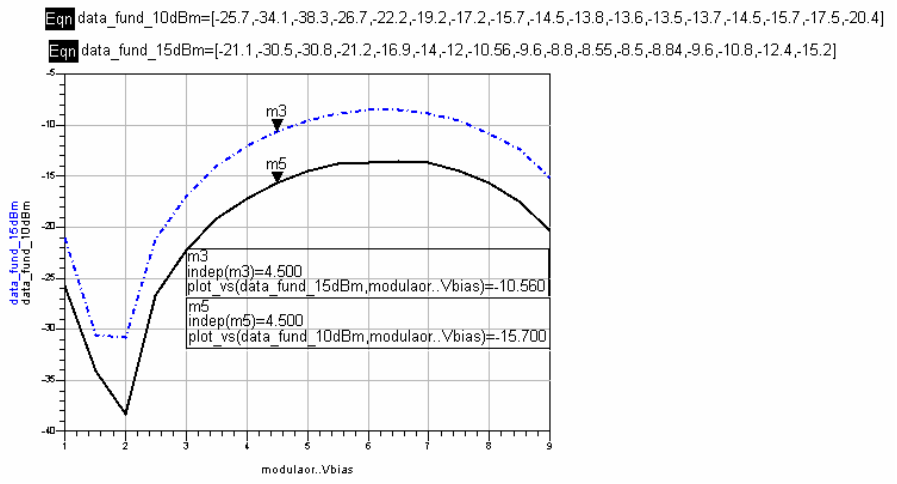

a) The fundamental tone

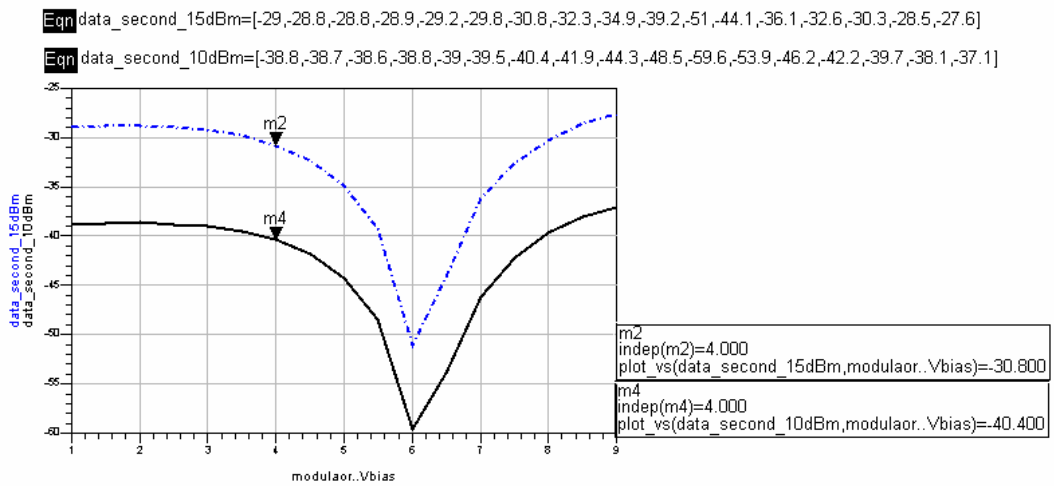

b) The second harmonic

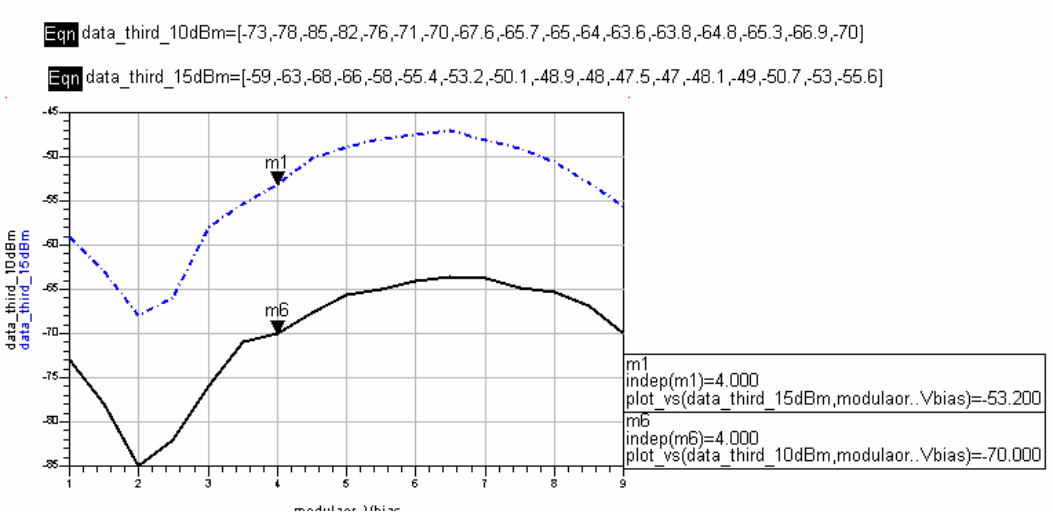

c) the third harmonic

Figure 4.11 Harmonics for 10 dBm and 15 dBm inputs

4.5.5 Spectrum:

The spectrum calculated in the ADS and taken from the data setup for the input power 10 dBm are shown in the two plots given in Figure 4.12

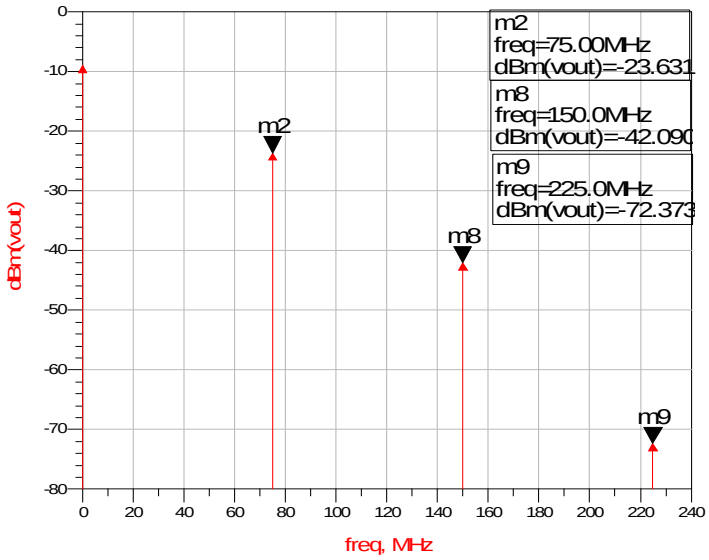

a) Simulation result

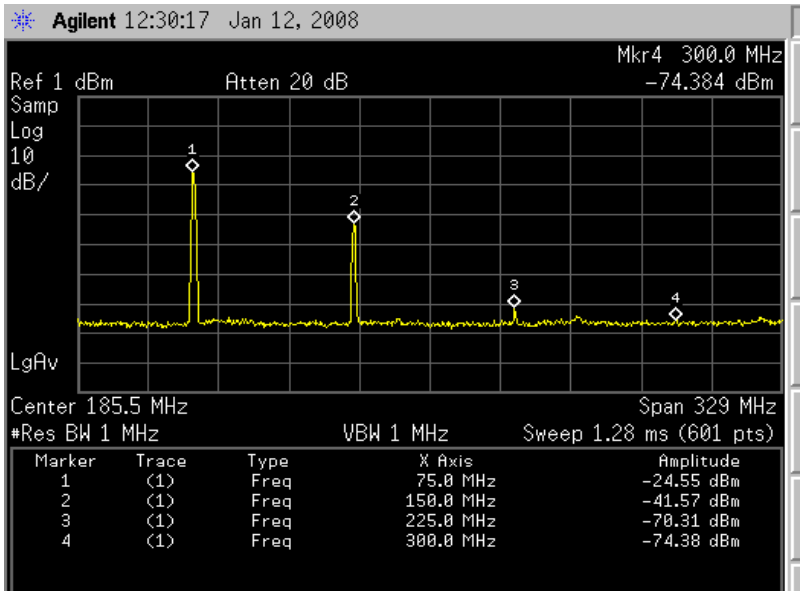

b) Output of spectrum analyzer

Figure 4.12 Spectrum at the output of the modulator

4.6 Two Tone Modulation

From the formula given in section 4.3 the amplitude of the fundamental term is

$$I_{fund} = I_{input} \times J_1\left(\pi \frac{V_1}{V_\pi}\right) J_0\left(\pi \frac{V_1}{V_\pi}\right) \sin\left(\pi \frac{V_{DC}}{V_\pi}\right) \quad (4.17)$$

So the corresponding power is given by

$$P_{fund} = C_2 + 20\log_{10}\left(J_1\left(\pi \frac{V_1}{V_\pi}\right) J_0\left(\pi \frac{V_1}{V_\pi}\right) \sin\left(\pi \frac{V_{DC}}{V_\pi}\right) \right) \quad (4.18)$$

Where C_2 is some proportionality constant

The sum (and difference) frequency of the two input frequencies has the power

$$P_{difference} = C_2 + 20\log_{10}\left(J_1\left(\pi \frac{V_1}{V_\pi}\right) J_1\left(\pi \frac{V_1}{V_\pi}\right) \cos\left(\pi \frac{V_{DC}}{V_\pi}\right) \right) (4.19)$$

And the second harmonic component has the power

$$P_{second} = C_2 + 20\log_{10}\left(J_2\left(\pi \frac{V_1}{V_\pi}\right) J_0\left(\pi \frac{V_1}{V_\pi}\right) \cos\left(\pi \frac{V_{DC}}{V_\pi}\right) \right) (4.20)$$

Following ADS schematic is constructed in order to simulate the system. Also the formulas given above and data taken from the setups are plotted in the graphs in the ADS to allow comparison.

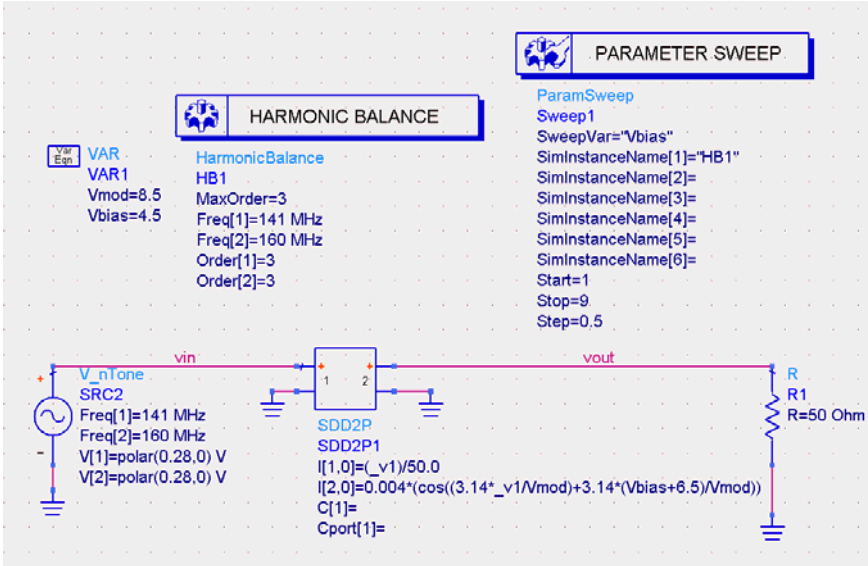

Figure 4.13 Simulation setup to analyze the two tone system

For two tone modulation an RF combiner is introduced to the setup. Since the loss in the combiner is 10 dB, and 2.5 dB is lost in the isolators, when the generators are set to 10 dBm the input power to the isolator becomes -2.5 dBm. Which is

$$10^{-\frac{2,5}{10}} = 0,56\,\text{mW}$$

Which corresponds to

$$\frac{V_{rms}{}^{2}}{50} = 0,00056 \Rightarrow V_{rms} = 0,167\ \text{Volts on 50 ohms}$$

The peak value is 0,167*1,414=0,24 Volts. In the ADS the value of the input voltage that fits best to practical values is found to be 0,28 Volts.

For two tone modulation, the power levels seen in the spectrum analyzer along with the theoretically calculated levels is given in the graphs given below.

4.6.1 The Fundamental Term:

For the fundamental tone, the graph of the data taken (solid line) and curve obtained from the formula is given in the figure below

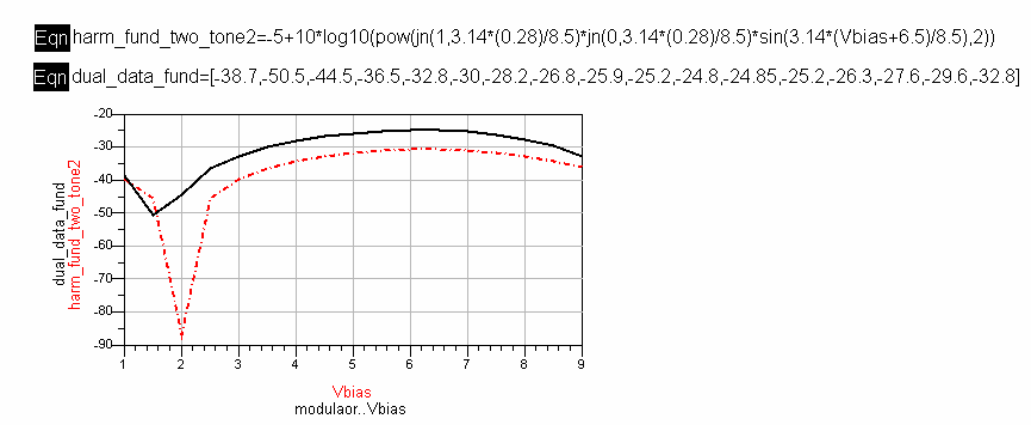

Figure 4.13 Fundamental term (two-tone) versus DC Bias

4.6.2 The Difference Term:

For the difference component, the graph of the data taken (solid line) and curve obtained from the formula is given in Figure 4.14

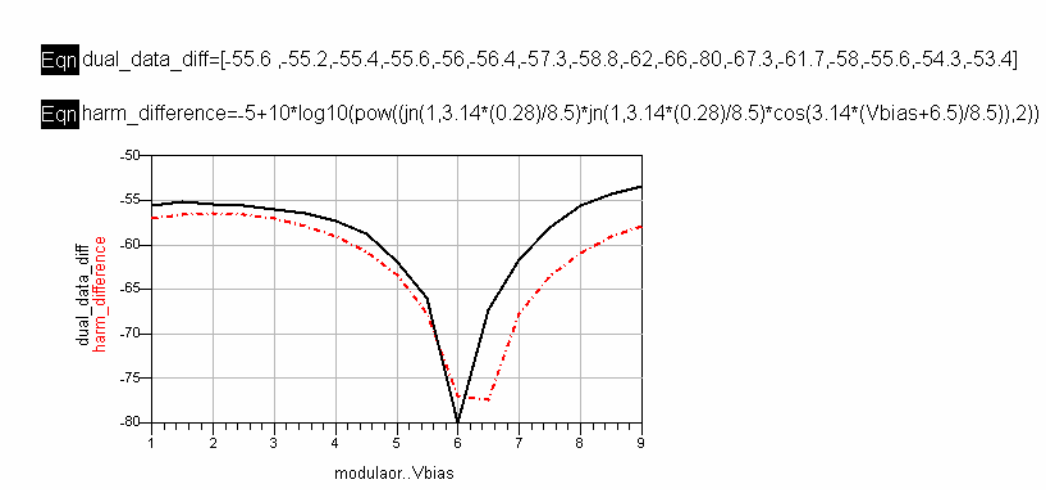

Figure 4.14 Difference term versus DC Bias

4.6.3 The Second Harmonic Term:

For the second harmonic component, the graph of the data taken (solid line) and curve obtained from the formula is given below

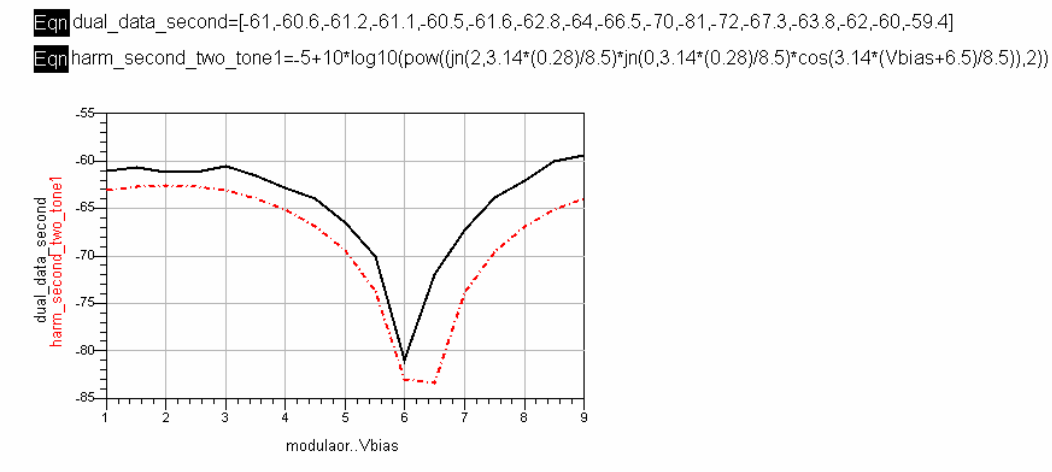

Figure 4.15 Second harmonic (two-tone) versus DC Bias

4.6.4 The Spectrum:

The spectrum calculated in the ADS and taken from the data setup are shown in the two plots given in Figure 4.16

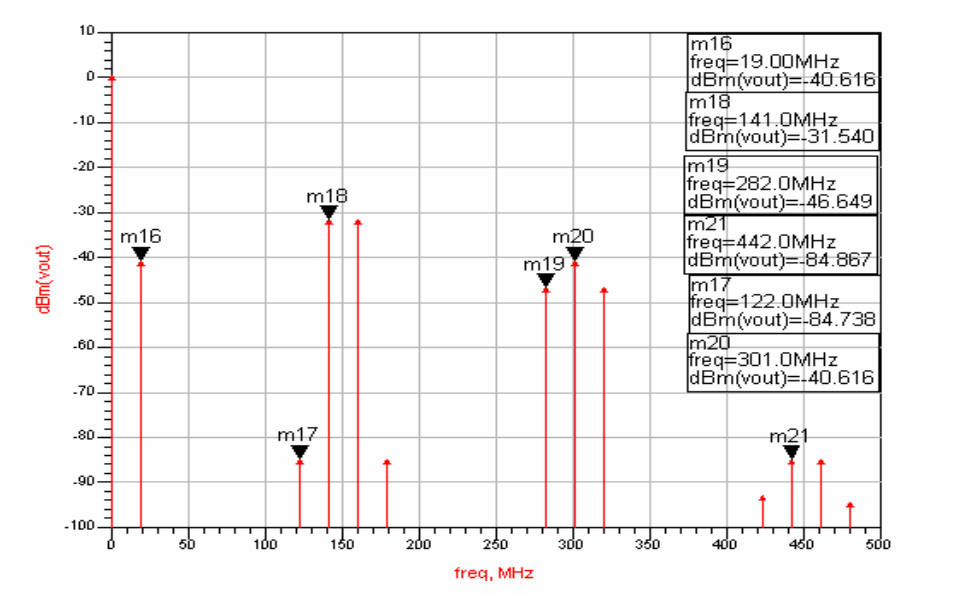

a) simulation results

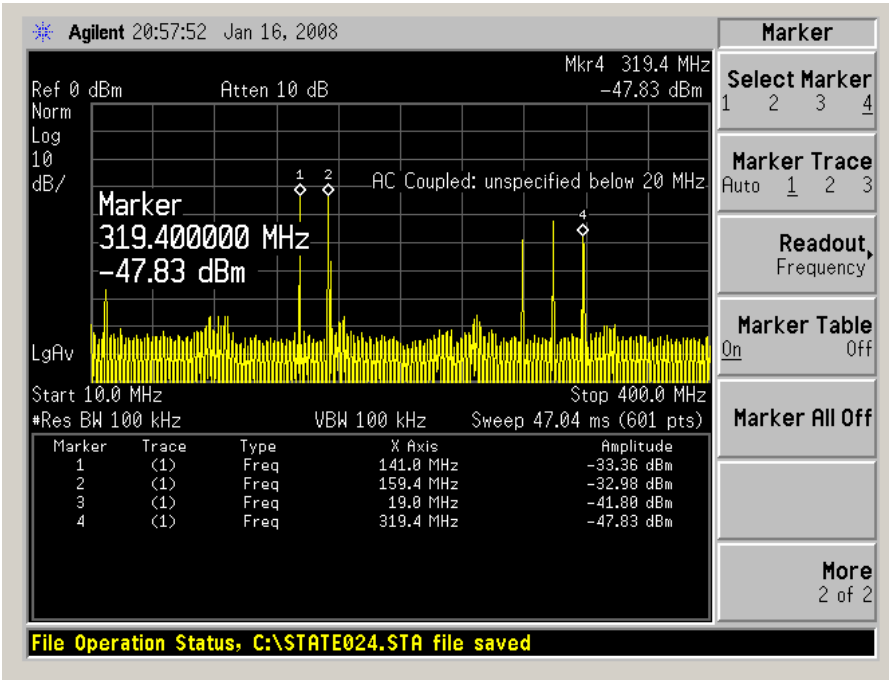

b) output of spectrum analyzer

Figure 4.16 The spectrum for two tone modulation a) simulation b) output of spectrum analyzer

Up till now only harmonics of a single tone or the mix of equal amplitude signals was considered. However in practical applications, the receiver path of a radio for example, the information carrying RF signal which has very low power is mixed with a relatively high power local oscillator (LO) to obtain IF signal.

Generally the LO signal is used the switch the RF signal on and off. The mixer utilizes some nonlinear elements, such as diodes, to convert RF to IF. Higher level of LO induces the nonlinearities of these devices easily and the performance of the mixer is improved.

A setup was constructed to observe the behavior of the modulator when a high level LO (around 22 dBm) is added to a low power RF signal (around -5 dBm). The modulator is biased at the point (1.9 V_{DC}) where the even harmonics are strongest and odd harmonics are weak. Also the two tap FIR filter constructed in chapter 1 was added to the output of the modulator to filter LO and RF frequencies. The power of the sum and difference frequencies $f_{LO}+f_{RF}$ and $f_{LO}-f_{RF}$, which are equal in amplitude, was observed.

The signal generators used (hp 8657A and Agilent E4434B) could not produce signal level of 22 dBm therefore a PA module (RA07H4047M of Mitsubishi) is utilized to obtain this level. Note that a level of 22 dBm on 50 ohms correspond to a voltage level around 8 Volts peak to peak which is close to V_{π} of the optical modulator.

The leakage of high power LO to the RF path is prevented by inserting filters on both the LO and RF paths. The LO frequency is selected as 354 MHz and the RF frequency is selected as 118 MHz since these are the frequencies where the two tap optical filter has notches. The constructed filters and combiner has the circuit schematic and response curves a given in Figure 4.17

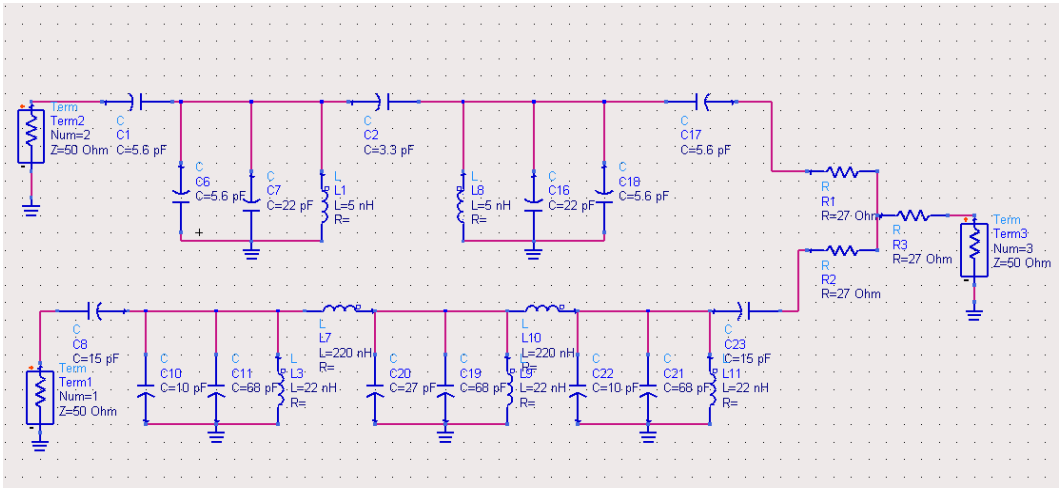

a) the schematic

b) the response of filter at 118 MHz (S31)

c) the response of filter at 354 MHz (S32)

Figure 4.17 The schematic and response curves for the combining circuitry

For the LO level of 22 dBm and RF level of -5 dBm the level of the difference frequency (and also the sum frequency) is found to be -28 dBm which correspond to a conversion loss of 23 dB. The power level of the output signal versus LO level and input signal level are plotted in Figure 4.18 a) and b) respectively

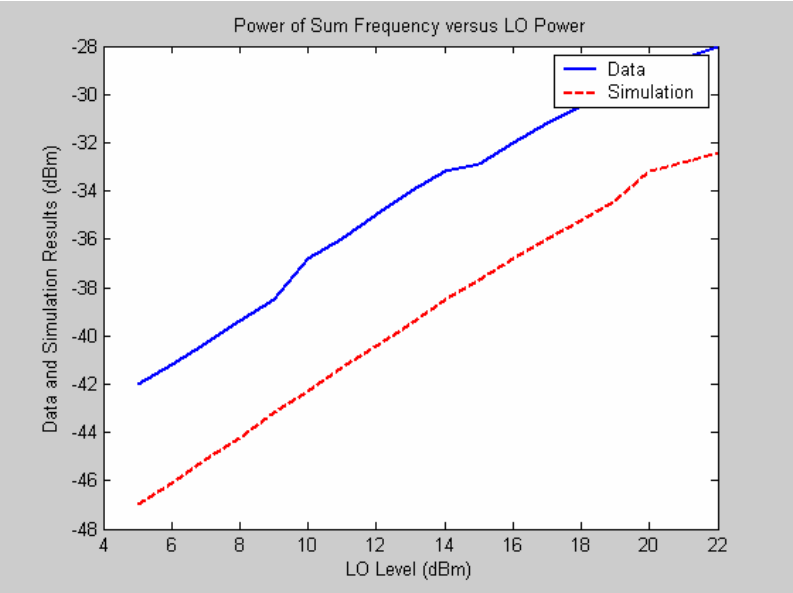

a) Difference Frequency power versus LO Level

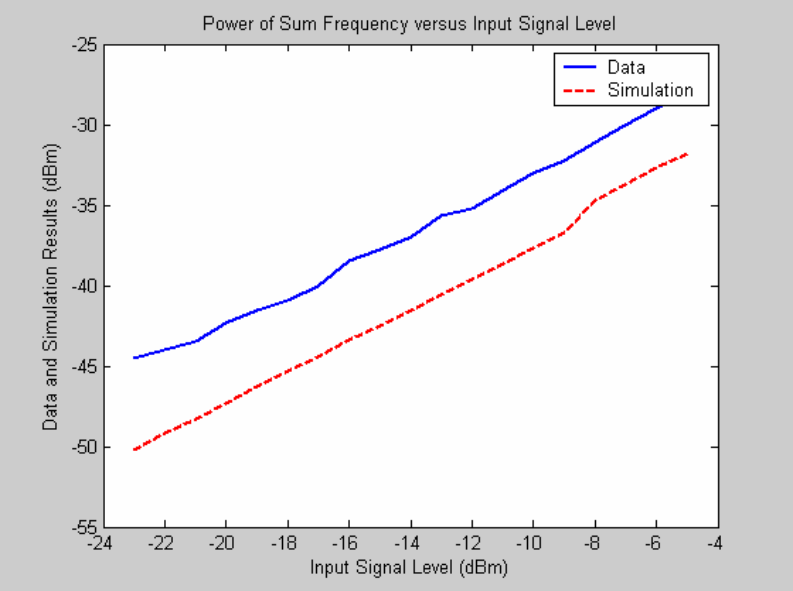

b) Difference Frequency power versus input signal level

Figure 4.18 Output Signal level versus a) LO Level
b) Input Signal Level

The picture of the setup used throughout the thesis is given in Figure 4.18

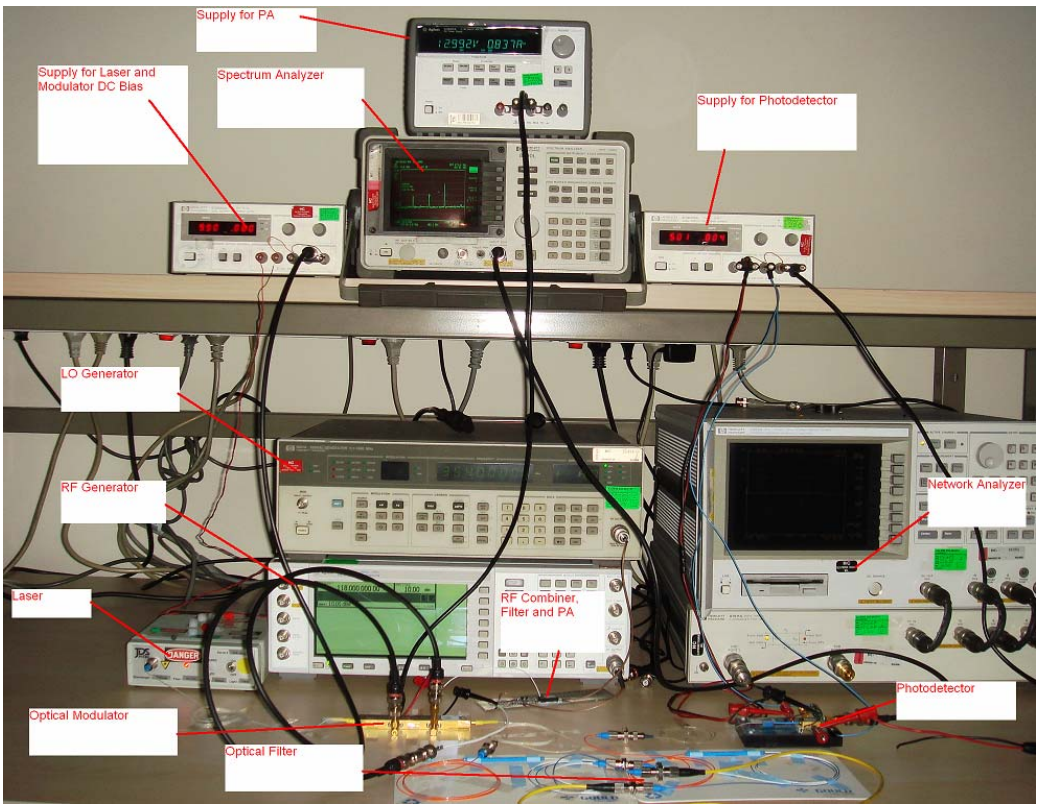

Figure 4.19 the picture of the setup

CHAPTER 5

CONCLUSIONS

In this thesis mixing and methods of filtering of microwave signals in optical domain is represented. Two photonic microwave filters are implemented (a FIR and an IIR) and their responses are compared with the Matlab simulation. Also harmonic mixing of microwave signals is achieved by the utilization of nonlinear properties of the $LiNbO_3$ optical modulator. The aim was to produce sum and difference frequencies of two microwave signals. Undesired harmonics are removed by using the previously constructed filter.

Chapter 2 includes filtering methods of microwave signals in optical domain. Both FIR filters and IIR filters are introduced and their responses are both derived and plotted. The advantages of using fiber cables as delay lines is explained. Also the disadvantages and limitations of photonic filters when compared with their microwave counterparts are mentioned.

Chapter 3 gives theoretical background about the photodetectors and lasers. The performance criteria for photodetectors are presented along with the explanation of the operation of PIN diode. Also operation principles of the lasers is introduced in this chapter.

The physical process utilized to achieve modulation of the optical carrier is explained in Chapter 4. This chapter also includes the experiments to analyze the nonlinearity of the modulator. The modulator is biased at different Q-points and the harmonics are observed for both single tone and two tone modulations. For

two tone modulation, emphasis is given to sum and difference frequencies and at the end of the chapter a system is constructed to create the sum frequency of two input signals. The two tap FIR filter constructed in Chapter 1 is also used to filter the unwanted frequency components.

Some concluding remarks for this thesis about the generation of the sum and difference frequencies may be presented as follows.
During the design of the filters a difficulty that was observed is the instability of the response of the filters. Although these filters are incoherent filters, the response seen on the network analyzer show fluctuations which is the sign for instability. This problem is partially solved by providing an environment with relatively stable temperature and using polarization controllers.

The phase induced intensity noise (PIIN) of the filter was around -50 dBm when measured at a resolution bandwidth of 3 MHz. This correspond to a noise level of -115 dBm/Hz which limits the usage of this filter in high sensitivity applications. The methods to reduce the PIIN noise could not be applied simply because the required components were not available.

Another aspect to be considered is the utilization of RF filters before applying the RF and LO signals to the optical modulator. One may claim that if one is able to construct those filters at high frequencies then photonic filters are not required at all. Note however that these filters are utilized to prevent the feedthrough between the LO and RF paths. Hence these filters can be removed by applying the RF and LO signals to the different arms of the optical modulator. The reason why we did not do this is the damaged second arm of the modulator.

The aforementioned conversion loss (around 23 dB) of the frequency converter may seem large when compared with the performance of the RF mixers which have conversion loss values about 5-10 dB. However increasing the power of the laser source will reduce the loss of the frequency converter, even gain can be obtained at higher power levels. Unfortunately high power lasers also require highly linear photodetectors which was not available to us. Also the bandwidth

of the photodetector (around 1 GHz) limited our highest RF and LO frequencies.

The sum and difference frequencies are obtained at a modulator bias where even harmonics are strongest. This situation also lead to a strong second harmonic of the LO frequency (708 MHz) which does not coincide with one of the notches of the photonic filter. To eliminate this component one may utilize another photonic filter.

As a conclusion this thesis dealt with the construction of a down converter by using an optical modulator and a photonic filter. The data taken from the setup are compared with the simulation results and coherence between the two is observed.

THE REFERENCES

[1] A. Seeds, “Microwave photonics,” IEEE Trans. Microwave Theory Tech., vol. 50, pp. 877–887, 2002.

[2] J. Capmany, B. Ortega, D. Pastor, and S. Sales, “Discrete-time optical processing of microwave signals,” J. Lightw. Technol., vol. 23, no. 2, pp. 702–723, Feb. 2005.

[3] R. A. Minasian, K. E. Alameh, and E. H. W. Chan, “Photonics-based interference mitigation filters,” IEEE Trans. Microwave Theory Tech., vol. 49, pp. 1894–1899, 2001.

[4] K. Wilner and A. P. van den Heuvel, “Fiber-optic delay lines for microwave signal processing,” Proc. IEEE, vol. 64, p. 805, 1976.

[5] EE-627 Principles of Modern Optical Systems, Lecture Notes
Gonul Turhan Sayan, METU

[6] EE-755 Infrared Devices and Systems, Lecture Notes
Cengiz Besikci, METU

[7] K. Jackson, S. Newton, B. Moslehi, M. Tur, C. Cutler, J. Goodman, and H. J. Shaw, “Optical fiber delay-line signal processing,” IEEE Trans. Microw. Theory Tech., vol. MTT-33, no. 3, pp. 193–204, Mar. 1985.

[8] Richard G. Lyons, Understanding Digital Signal Processing
Prentica Hall PTR Publication

[9] J. Capmany, J. Mora, B. Ortega, and D. Pastor, “High Q microwave photonics filter using a tuned modulator,” Opt. Lett., vol. 30, no. 17, pp. 2299–2301, Sep. 2005

[10] “High-Q optical microwave filter,” Electron. Lett., vol. 35, no. 24, pp. 2125–2126, Nov. 1999.

[11] M. Tur, B. Moslehi, and J. Goodman, “Theory of laser phase noise in recirculating fiber-optic delay lines,” J. Lightw. Technol., vol. LT-3, no. 1, pp. 20–31, Jan. 1985.

[12] B. Moslehi, “Analysis of optical phase noise in fiber-optic systems employing a laser source with arbitrary coherence time,” J. Lightw. Technol., vol. LT-4, no. 9, pp. 1334–1351, Sep. 1986.

[13] K. Petermann and G. Arnold, “Noise and distortion characteristics

of semiconductor lasers in optical fiber communication systems," IEEE J. Quantum. Electron., vol. QE-18, pp. 543-555, 1982.

[14] Robert A. Minasian, " Photonic Signal Processing of Microwave Signals" IEEE Transactions on Microwave Theory and Techniques, vol. 54, no. 2, February 2006

[15] Behzad Moslehi, "Noise Power Spectra of Optical Two-Beam Interferometers Induced by the Laser Phase Noise" JOURNAL OF LIGHTWAVE TECHNOLOGY, VOL. LT-4, NO. 11, NOVEMBER 1986

[16] J. Capmany, D. Pastor,A.Martinez, B. Ortega, and S. Sales, "Microwave photonic filters with negative coefficients based on phase inversion in an electro-optic modulator," Opt. Lett, pp. 1415–1417, 2003.

[17] E. H. W. Chan and R. A. Minasian "Novel all-optical RF notch Filters with equivalent negative tap response," IEEE Photon. Technol. Lett., vol. 16, no. 5, pp. 1370–1372, May 2004.

[18] W. Zhang, J. A. R. Williams, and I. Bennion, "Optical fiber delay line filter free of the limitation imposed by optical coherence," Electron. Lett., vol. 35, pp. 2133–2134, 1999.

[19] E. H. W. Chan and R. A. Minasian, "Photonic notch filter without optical coherence limitations," J. Lightw. Technol., vol. 22, no. 7, pp. 1811–1817, Jul. 2004.

[20] A. Ho-Quoc, S. Tedjini, and A. Hilt, "Optical polarization effect in discrete time fiber-optic structures for microwave signal processing," in IEEE MTT-Symp. Dig., San Francisco, CA, 1996, pp. 907–910.

[21] B. Vidal, V. Polo, J. L. Corral, and J. Marti, "Photonic microwave filter with tuning and reconfiguration capabilities using optical switches and dispersive media," Electron. Lett., vol. 39, no. 6, pp. 547–548, Mar. 2003.

[22] J. Capmany, D. Pastor, B. Ortega, " A Tutorial on Microwave Photonic Filters" Journal of Lightwave Technology. vol.24 no.1 2006

[23] N. You and R. A. Minasian, "A novel high-Q optical microwave processor using hybrid delay line filters," IEEE Trans. Microwave Theory Tech., vol. 47, pp. 1304–1308, 1999.

[24] J. Capmany, D. Pastor, and B. Ortega, “New and flexible fiber-optic delay line filters using chirped Bragg gratings and laser arrays,” IEEE Trans. Microw. Theory Tech., vol. 47, no. 7, pp. 1321–1327, Jul. 1999.

[25] Govind P. Agraval, “Fiber Optic Communication Systems”, Willey Interscience

[26] Philip C. D. Hobbs, “Building Electro-Optical Systems: Making it All Work”, Copyright 2000 John Wiley & Sons, Inc.

[27] Moal C. Gupta, John Bollato, “Handbook of Photonics” ,CRC Press 2007

[28] Amnon Yariv, Pochi Yeh, “ Optical Electronics in Modern Communications”, Oxford University Press 2007

[29] Muhammad Taher Abuelma’atti, “Large Signal Analysis of the Mach-Zender Modulator with Variable Bias” Proc. Natl. Sci. Counc. ROC(A), Vol. 25, No 4, 2001. pp. 254-528

[30] O. Mitomi, K. Noguchi, H. Miyazawa. “ Estimation of frequency response for high-speed $LiNbO_3$ optical modulators” IEE Proc.-Optoelectron. Vol. 146, No 2, April 1999

APPENDIX A

In this appendix the data sheet of the Optical modulator used in the experiments is given.

agere systems

Data Sheet
May 2001

10 Gbits/s Lithium Niobate Electro-Optic Modulator

The Lithium Niobate Modulators include three single-drive modulators (2623N, 2623Y, 2623CS) and a single-drive modulator with an integrated attenuator (2623CSA). All devices are capable of modulation rates up to 10 Gbits/s.

Features

- Ti-diffusion process
- Single-drive technology
- C- and L-band models
- Slim, hermetic package
- Bandwidths up to 10 GHz
- Operational over a temperature range of 0 °C to 70 °C
- 43 Ω design for minimal electrical reflections
- Angled interfaces for minimal optical reflections
- Integrated optical attenuator available on 10 Gbits/s modulator (2623CSA)
- Tested to *Telcordia Technologies** 468

Benefits

- Excellent long-term bias stability
- Internal polarizer
- Low modulation voltages

Applications

- Digital high-speed telecommunications:
  — SONET: OC-1 through OC-192
  — SDH: STM-16, STM-64
  — Undersea communications
- Internet data communications
- SONET/SDH test equipment

Optical/Electrical Characteristics (continued)

Electrical Signal Input

Electrical signal input is made through SMA coaxial connectors. The standard device includes an internal termination network. Care must be taken not to exceed the recommended 8 in./lb. of torque when making connections to these inputs. High-frequency coaxial cable is recommended.

Characteristic Curves

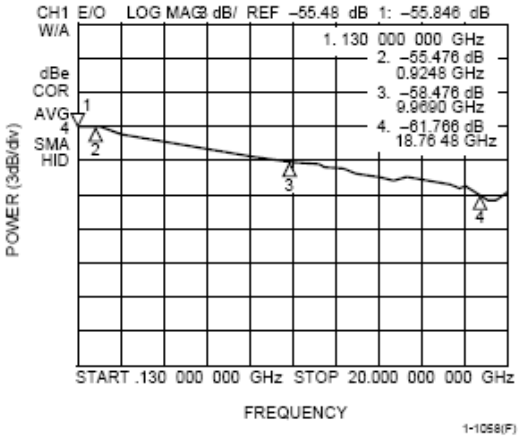

Figure 3. Magnitude of Electro-Optic Response, 0.130 GHz—20 GHz.

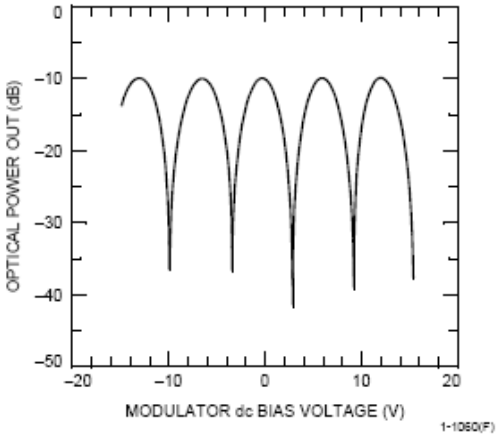

Figure 5. Output Power vs. Bias Voltage

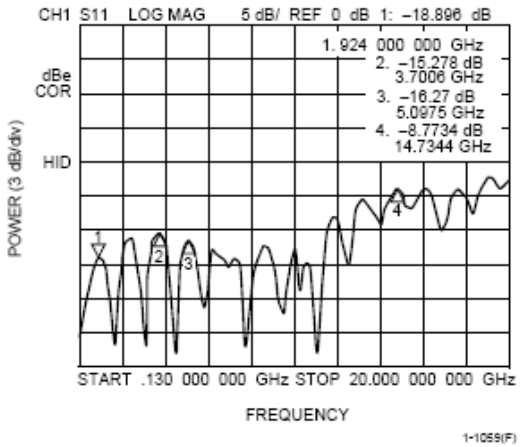

Figure 4. S11, 0.130 GHz—20 GHz

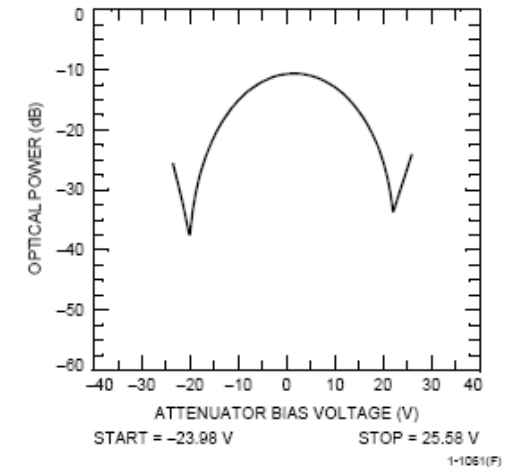

Figure 6. Optical Power vs. Attenuator Bias Voltage

APPENDIX B

In this appendix the data sheet of the power amplifier module, which used in the experiments is given.

ELECTROSTATIC SENSITIVE DEVICE
OBSERVE HANDLING PRECAUTIONS

MITSUBISHI RF MOSFET MODULE

RA07H4047M

400-470MHz 7W 12.5V PORTABLE/ MOBILE RADIO

DESCRIPTION

The RA07H4047M is a 7-watt RF MOSFET Amplifier Module for 12.5-volt portable/ mobile radios that operate in the 400- to 470-MHz range.

The battery can be connected directly to the drain of the enhancement-mode MOSFET transistors. Without the gate voltage (V_{GG}=0V), only a small leakage current flows into the drain and the RF input signal attenuates up to 60 dB. The output power and drain current increase as the gate voltage increases. With a gate voltage around 2.5V (minimum), output power and drain current increases substantially. The nominal output power becomes available at 3V (typical) and 3.5V (maximum). At V_{GG}=3.5V, the typical gate current is 1 mA.
This module is designed for non-linear FM modulation, but may also be used for linear modulation by setting the drain quiescent current with the gate voltage and controlling the output power with the input power.

FEATURES

- Enhancement-Mode MOSFET Transistors (I_{DD}≅0 @ V_{DD}=12.5V, V_{GG}=0V)
- P_{out}>7W @ V_{DD}=12.5V, V_{GG}=3.5V, P_{in}=20mW
- η_T>40% @ P_{out}=7W (V_{GG} control), V_{DD}=12.5V, P_{in}=20mW
- Broadband Frequency Range: 400-470MHz
- Low-Power Control Current I_{GG}=1mA (typ) at V_{GG}=3.5V
- Module Size: 30 x 10 x 5.4 mm
- Linear operation is possible by setting the quiescent drain current with the gate voltage and controlling the output power with the input power

BLOCK DIAGRAM

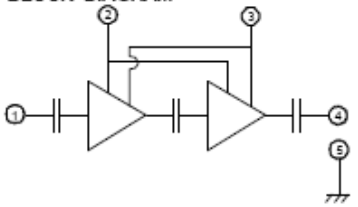

1. RF Input (P_{in})
2. Gate Voltage (V_{GG}), Power Control
3. Drain Voltage (V_{DD}), Battery
4. RF Output (P_{out})
5. RF Ground (Case)

APPENDIX C

In this appendix the data sheet of the Optical Beam Combiner/Splitter used in the experiments is given.

Polarization Beam Combiner/Splitter

PBC/S–001

The PBC/S-001 can be used either as a polarization beam combiner to combine light beams from two PM input fibers into a single output fiber, or as a polarization beamsplitter to split light from an input fiber into two output fibers of orthogonal polarization states. An important application of this device is polarization division multiplexing or demultiplexing in optical systems to increase their transmission capacity. In addition, as a pump combiner in optical amplifiers, the device efficiently combines the output from two pump lasers into a single fiber to increase the optical amplifier's saturation power and to reduce its polarization sensitivity. The wide operation bandwidth and high power handling capability (up to 2000 mW) make the device very attractive for next-generation amplifier systems. Finally, with a rugged stainless package designed for high optical performance and stability, this compact device offers low excess insertion loss, low back reflection, and high extinction ratio that equal or surpass others on the market.

Specifications

Common port fiber option	SM	PM
Insertion Loss	0.3 dB	0.4 dB typical 0.6 dB max.
Extinction Ratio (ER) (PBS only)	23 dB	22 dB
Center Wavelength	1460nm, 1480nm, 1550nm*	1310nm, 1480nm, 1550nm
Operating Bandwidth	± 30 nm	±40 nm
Return Loss	50 dB	50 dB
Optical Power Handling	2000 mW	500 mW
Operating Temperature	0° to 70° C	-5° to 70° C
Storage Temperature	-40° to 85° C	-40° to 85° C
Dimensions	Ø 5.5 x 30 mm	Ø 5.5 x 35 mm
Fiber Type	Port 1: SMF 28	Port 1: PM Panda Fiber
	Port 2 and Port 3: PM Panda Fiber	

Note: Values are referenced without connectors.

Applications:

- Polarization division Mux/DeMux
- EDFA and Raman Amplifiers
- Instrument
- R&D Laboratories

Unique Features:

- Compact
- Low Insertion Loss
- Rugged Design
- High Power Handling